

# Optimising Spatial and Tonal Data for PDE-based Inpainting\*

Laurent Hoeltgen, Markus Mainberger, Sebastian Hoffmann, Joachim Weickert, Ching Hoo Tang, Simon Setzer, Daniel Johannsen, Frank Neumann, and Benjamin Doerr

<sup>1</sup> L. Hoeltgen

Faculty of Mathematics, Natural Sciences and Computer Science, Brandenburg Technical University Cottbus–Senftenberg, 03046 Cottbus, Germany

`hoeltgen@b-tu.de`

<sup>2</sup> M. Mainberger

<sup>3</sup> S. Hoffmann

<sup>4</sup> J. Weickert

<sup>5</sup> S. Setzer

Mathematical Image Analysis Group, Faculty of Mathematics and Computer Science, Campus E1.7, Saarland University, 66041 Saarbrücken, Germany

`{mainberger, hoffmann, weickert, setzer}`

`@mia.uni-saarland.de`

<sup>6</sup> C. H. Tang

Research Group 1: Automation of Logic, Max Planck Institute for Informatics, Campus E1.4, 66123 Saarbrücken, Germany

`chtang@mpi-inf.mpg.de`

<sup>7</sup> D. Johannsen

School of Mathematical Sciences, Tel Aviv University, Ramat Aviv, Tel Aviv 69978, Israel

`mail@danieljohannsen.net`

<sup>8</sup> F. Neumann

School of Computer Science, Innova21 Building, University of Adelaide, Adelaide, SA 5005, Australia

`frank@cs.adelaide.edu.au`

<sup>9</sup> B. Doerr

LIX, 1 rue Honoré d'Estienne d'Orves, Bâtiment Alan Turing, Campus de l'École Polytechnique, CS35003, 91120 Palaiseau, France

`doerr@lix.polytechnique.fr`

---

\* Partly funded by the Deutsche Forschungsgemeinschaft (DFG).



**Abstract.** Some recent methods for lossy signal and image compression store only a few selected pixels and fill in the missing structures by inpainting with a partial differential equation (PDE). Suitable operators include the Laplacian, the biharmonic operator, and edge-enhancing anisotropic diffusion (EED). The quality of such approaches depends substantially on the selection of the data that is kept. Optimising this data in the domain and codomain gives rise to challenging mathematical problems that shall be addressed in our work.

In the 1D case, we prove results that provide insights into the difficulty of this problem, and we give evidence that a splitting into spatial and tonal (i.e. function value) optimisation does hardly deteriorate the results. In the 2D setting, we present generic algorithms that achieve a high reconstruction quality even if the specified data is very sparse. To optimise the spatial data, we use a probabilistic sparsification, followed by a nonlocal pixel exchange that avoids getting trapped in bad local optima. After this spatial optimisation we perform a tonal optimisation that modifies the function values in order to reduce the global reconstruction error. For homogeneous diffusion inpainting, this comes down to a least squares problem for which we prove that it has a unique solution. We demonstrate that it can be found efficiently with a gradient descent approach that is accelerated with fast explicit diffusion (FED) cycles. Our framework allows to specify the desired density of the inpainting mask a priori. Moreover, is more generic than other data optimisation approaches for the sparse inpainting problem, since it can also be extended to nonlinear inpainting operators such as EED. This is exploited to achieve reconstructions with state-of-the-art quality.

Apart from these specific contributions, we also give an extensive literature survey on PDE-based image compression methods.

**Keywords:** Inpainting, Image Compression, Optimisation, Free Knot Problem, Diffusion, Partial Differential Equations (PDE's), Interpolation, Approximation

**Mathematics Subject Classification (2000)** MSC 94A08, MSC 65Nxx, MSC 65Kxx

## 1 Introduction

One of the most fascinating properties of variational methods and partial differential equations (PDE's) in image analysis is their property to fill in missing data. This filling-in effect has a long tradition: It can be found already in the seminal optic flow paper of Horn and Schunck [67], where the smoothness term propagates information to regions in which the data term is small or even vanishes. More explicit interpolation ideas are exploited in so-called inpainting approaches. They go back to Masnou and Morel [94], became popular by the work of Beltalmío *et al.* [9], and have been modified and extended by many others such as [12, 24, 60, 134]. Inpainting problems arise when certain parts of the image domain are degraded in such a way that any useful data is unavailable. In the remaining parts of the image domain, the data is available and undegraded. The goal is to reconstruct the missing information by solving a suitable boundary value problem where the data in the undegraded regions serve as Dirichlet boundary conditions.

PDE-based image compression methods constitute a challenging application area of inpainting ideas; see Section 2 for a detailed review and many

references. These lossy compression approaches drive inpainting to the extreme: They store only a very small fraction of the data and inpaint the missing data with a suitable differential operator. However, PDE-based compression differs fundamentally from classical inpainting by the fact that it has the liberty to select the data that is kept. Typically one specifies only that a certain fraction of the image data is stored, and the codec<sup>10</sup> can optimise this data in order to minimise the reconstruction error. Obviously this involves a spatial optimisation step that selects the locations of the kept pixels. We call these locations the *inpainting mask*. Interestingly, it may also be beneficial to optimise the grey values of the selected pixels: While changing the grey values deteriorates the approximation quality inside the mask, it can improve the approximation in the (usually much larger) inpainting domain where no data is specified. This grey value optimisation is also called *tonal optimisation*.

In order to judge the potential of PDE-based compression approaches, it is important to go to the extreme and find the limits that inpainting with optimised sparse data can offer. This should include both spatial and tonal optimisation for different inpainting operators. In a first step, it can make sense to have a clear focus on quality and postpone considerations of computational efficiency and coding costs to later work when the quality questions are answered in a satisfactory way.

Following this philosophy, the goal of our contribution is to explore the potential of PDE-based inpainting of sparse data that can be optimised both spatially and tonally. In order to evaluate different inpainting operators in a fair way, we aim at algorithms that are as generic and widely applicable as possible, and we optimise quality rather than speed. Computation time becomes only relevant for us when different methods lead to identical results. First our insights and algorithms are derived in more restricted settings. Afterwards, we investigate how these ideas can be extended and generalised.

Our work is organised as follows. We start by presenting a survey on PDE-based image compression in Section 2. Afterwards we discuss the homogeneous diffusion inpainting framework that is used for most of our optimisation algorithms in this work. In Section 4, we present methods that aim at optimal spatial and greyvalue data for homogeneous diffusion interpolation in 1D. The subsequent Section 5 deals with optimisation strategies in 2D. In Section 6, we present extensions to higher order and nonlinear diffusion inpainting operators. Finally we conclude with a summary in Section 7.

Our discussions are based on a conference paper [91], in which we have introduced probabilistic sparsification and tonal optimisation for homogeneous diffusion inpainting. Here we extend these results in a number of ways. Our main innovations are:

1. We present a new section that gives a detailed review of PDE-based image compression methods. Since this area has developed in a very fruitful

---

<sup>10</sup> A codec is a system for image coding and decoding.

way and no review article is available so far, we feel that such a review section can be a useful starting point for readers who would like to learn more on this topic.

2. In another new section we derive a mathematically sound approach to solve the data optimisation problem for homogeneous diffusion inpainting of strictly convex signals in 1D. This restricted 1D setting allows us to gain insights into the nonconvexity of the problem and to quantify the errors that are caused by separating spatial and tonal optimisation.
3. We introduce a new algorithm for tonal optimisation, based on a gradient descent approach with an acceleration by a fast explicit diffusion (FED) strategy. While it achieves the same quality as previous approaches, we show that it is more efficient.
4. We explain how to extend our methods to more advanced linear or non-linear inpainting operators such as biharmonic inpainting and inpainting by edge-enhancing anisotropic diffusion. In this way we achieve sparse PDE-based reconstructions of hitherto unparalleled quality.

## 2 A Review of PDE-Based Image Compression

Before describing our approach on spatial and tonal data optimisation in the forthcoming sections, we first review existing approaches to PDE-based image compression. These methods belong to the class of lossy compression techniques. Hence, they aim at finding very compact file representations such that the resulting reconstructions approximate the original image well.

PDE-based approaches are alternatives to established transform-based codecs such as the JPEG standard [104] which uses the discrete cosine transform (DCT), or its successor JPEG 2000 [126] that involves the wavelet transform. However, since they follow a completely different concept, it is worthwhile to give an overview of their various aspects.

To this end, we review data optimisation questions, the choice of appropriate inpainting operators, and strategies to store the optimised data efficiently. Afterwards we describe PDE-based codecs that are based on specific image features, and we discuss algorithmic aspects, variants and extensions, as well as relations to other approaches.

Our review focuses on methods that use PDE's as a main tool for compression. This means that we do not discuss the numerous PDE-based or variational techniques that have been advocated as a preprocessing step before coding images or videos (see e.g. [78, 128]) or as a postprocessing tool for removing coding artifacts (such as [3, 16, 52]).

### 2.1 Data Optimisation

Galić *et al.* [53, 54] have pioneered research on data selection methods for PDE-based image compression by proposing a subdivision strategy that inserts mask points at locations where the approximation error is too large.

While these authors used a triangular subdivision, Schmaltz *et al.* [118] modified this concept to rectangular subdivisions and added several algorithmic improvements that allowed them to beat the quality of JPEG 2000 with an anisotropic diffusion operator. Belhachmi *et al.* [8] have used the theory of shape optimisation to derive analytic results for the spatial optimisation problem in the case of homogeneous diffusion inpainting. Discrete approaches for the spatial and tonal optimisation problem with homogeneous diffusion inpainting have been presented by Mainberger *et al.* [91]. The spatial optimisation is based on a probabilistic sparsification strategy with nonlocal pixel exchange, while tonal optimisation is formulated as a linear least squares problem. Hoeltgen *et al.* [63] considered a control theoretic approach to the problem of data optimisation, also for homogeneous diffusion inpainting. They minimised the quadratic reconstruction error with a sparsity prior on the mask and a nonconvex inpainting constraint. Their numerical approach solves a series of convex optimisation problems with linear constraints. A similar constrained optimisation model was considered by Ochs *et al.* [101] who used this problem as a test scenario for their iPiano algorithm. Qualitatively both techniques gave similar results, but the iPiano approach offered advantages in terms of efficiency.

While all the before mentioned strategies pay much attention to spatial optimisation, less work has been devoted to tonal optimisation so far. Early heuristic attempts go back to Galić *et al.* [54]. They lifted the grey values up or down to the next quantisation levels in order to improve the approximation quality in the vicinity of the data. A first systematic treatment in terms of a least squares optimisation problem was given by Mainberger *et al.* [91], who used a randomised Gauß-Seidel algorithm. Faster numerical algorithms for the same problem have been proposed by Chen *et al.* [29], who applied the L-BFGS method, and by Hoeltgen and Weickert [64], who advocated the LSQR algorithm and a primal–dual technique.

## 2.2 Finding Good Inpainting Operators

Although many theoretical investigations on data selection methods are based on homogeneous diffusion inpainting, the task of finding better inpainting operators has been a research topic for a decade. Already in 2005, Galić *et al.* [53] have shown that edge-enhancing anisotropic diffusion (EED) [131] is better suited for PDE-based image compression than homogeneous diffusion. The favourable performance of anisotropic diffusion approaches of EED type has been confirmed by more detailed comparisons later on, both for randomly scattered data [14, 54] and for compression-optimised data [29, 118]. Some of these evaluations involve many other inpainting operators such as biharmonic interpolation [43] and its triharmonic counterpart, the absolute minimal Lipschitz extension [22], isotropic nonlinear diffusion [23, 105] and its approximations of total variation (TV) inpainting [26, 114], as well as

the inpainting operators of Bornemann and März [12] and of Tschumperlé [127]. Total variation inpainting performed consistently bad, showing that operators which work fairly well for denoising are not necessarily good for sparse inpainting. Biharmonic inpainting, on the other hand, turned out to be an interesting alternative to EED, when linearity or absence of any need for parameter specification are important, and over- and undershoots are acceptable.

### 2.3 Storing the Data

Besides finding sparse inpainting data that allow to approximate the original image in high quality, every practically useful codec must be able to store these data efficiently. Attempting this in a naive way would create a huge overhead, and the resulting codec would not be competitive to the quality that established transform-based codecs such as JPEG or JPEG 2000 can achieve for the same file size. The search for data that can be stored efficiently may even lead to compromises w.r.t. the data optimality: In order to use less bits, it is common to round the intensity values to a relatively small set of quantisation levels. Regarding the data localisation, it can be helpful to avoid a completely free configuration of data points and allow only masks which are represented efficiently with binary trees that result from subdivision strategies [53, 54, 118]. Moreover, also lossless entropy coders such as Huffman coding [68], JBIG [72], or PAQ [89] are highly useful to remove the redundancy of the data.

### 2.4 Feature-based Methods

Methods that rely on specific – often perceptually relevant – features rather than on data that are optimised for compression applications can be seen as predecessors or variants of PDE-based codecs. Let us now discuss the main types of such features and their relevance for coding.

**Contour-based Features** Edges are perceptually relevant features that have been analysed for a long time. Already in 1935, Werner [136] has investigated filling-in mechanisms from edges in biological vision systems. In computer vision, there are numerous approaches in scale-space and wavelet theory that attempt to reconstruct an image from its edge information [28, 32, 42, 45, 58, 69, 88, 93, 115, 142], often over multiple scales and supplemented with additional information.

Also within coding, publications that exploit information from edges or segment boundaries and combine it with inpainting processes have a long tradition [1, 7, 18, 21, 27, 36, 55, 57, 65, 80, 84, 87, 90, 137, 143]. However, for general images these features are often suboptimal as inpainting data. On the other hand, for specific applications where the images are piecewise constant or

piecewise smooth, such codecs can achieve competitive results. This includes cartoon-like images [90] or depth maps [27, 55, 65, 84]. For homogeneous diffusion inpainting and piecewise almost constant data, choosing data near edges can be justified by the theory of Belhachmi *et al.* [8]. It suggests to select the mask density as an increasing function of the Laplacian magnitude. Contour-based approaches also benefit from the fact that encoding of contour data is relatively inexpensive: One can use e.g. chain codes, and a smooth intensity variation along a contour allows subsampling without substantial quality degradations; see e.g. [90].

Related ideas are also advocated in computer graphics for image editing and vectorised image representations [46, 70, 102, 103]. Moreover, contour-based codecs that rely on inpainting processes with PDE's have been used successfully for encoding digital elevation maps [48, 121, 138], where information is available in terms of level lines.

**Point-based Features** In order to end up with more compact image representations, it appears tempting to consider point-based features instead of contour-based ones. Also here several results can be found in the literature.

Johansen *et al.* [71] and Kanters *et al.* [74] have performed research on reconstructing images from their top points in scale-space. Lillholm *et al.* [85] present more general discussions on how to reconstruct an image from a suitable set of feature points and their derivatives (local jet). More recently, also reconstruction attempts are described that are based on SIFT features [135] or local binary descriptors [33].

So far, all image reconstructions from isolated feature points that allow some perceptual interpretations or have shown their merits in other applications such as image matching do not offer a quality level that is sufficient for compression applications. It appears that these features are too sparse while lacking optimality.

## 2.5 Fast Algorithms and Real-Time Aspects

In real-time applications, the efficiency of a codec becomes a central criterion. Here one should distinguish between real-time capabilities during encoding and real-time decoding. Often the latter one is more important: For instance, when a company encodes a movie, it is acceptable if the creation of an optimised file takes many hours, as long as the customer is able to decode it in real-time.

On the encoding side, the approach of Belhachmi *et al.* [8] is algorithmically sufficiently simple to allow real-time performance: It computes the Laplacian magnitude of a Gaussian-smoothed image and converts the result to a inpainting binary mask by means of a halftoning method such as Floyd–Steinberg dithering [51]. Also the codec of Mainberger *et al.* [90] is of comparable computational simplicity. Most other approaches are not real-time



capable during encoding since they apply a sophisticated optimisation of data and parameters. However, also for data optimisation, substantial algorithmic accelerations have been achieved recently [64, 101].

On the decoder side, no time-consuming optimisation steps are required, and the main computational effort for PDE-based codecs consists of solving an inpainting problem. Thus, real-time decoding is possible if one uses appropriate algorithms and exploits the capabilities of modern hardware. In 2007, Köstler *et al.* [79] presented real-time algorithms for the subdivision approach of Galic *et al.* [53]. With multigrid methods for homogeneous diffusion inpainting or lagged diffusivity multilevel approaches for anisotropic diffusion inpainting, they could process more than 25 greyscale images per second of size  $320 \times 240$  on a Sony PlayStation 3. Also Mainberger *et al.* [90] proposed a multigrid approach for their edge-based homogeneous diffusion codec. On a PC CPU they reported runtimes around 6 frames per second for decoding a  $256 \times 256$  colour image. This is about 6 times higher than JPEG 2000 and 24 times higher than JPEG. For linear inpainting problems with very sparse data, algorithms based on discrete Green's functions can be an interesting alternative to multigrid methods [66]. Recently, Peter *et al.* [106] managed to decode 25 greyscale images per second with VGA resolution  $640 \times 480$  by means of anisotropic diffusion inpainting on a PC architecture with GPU support. This was accomplished with so-called FED schemes [59] that are well-suited for parallel implementations.

## 2.6 Hybrid Image Compression Methods

The usefulness of embedding inpainting concepts into existing transform-based image compression methods is studied in a number of publications [87, 111, 130, 139, 140]. Their goal is to benefit simultaneously from the advantages of inpainting methods and transform-based codecs. While PDE-based inpainting approaches often perform better at edges, transform-based codecs are favoured inside the regions, in particular if they are dominated by texture. By construction, such hybrid methods restrict themselves to the main application fields of both paradigms rather than pushing inpainting ideas to the limit.

An example of a hybrid approach that remains entirely within the inpainting framework is [108]. It combines EED-based inpainting with the sparse, exemplar-based approach of Facciolo *et al.* [47]. This results in a more faithful recovery of textured regions than a pure EED-based method.

Chan and Zhou [25] have proposed a hybrid method that modifies wavelet-based image compression by a TV regularisation of the wavelet coefficients. More recently, Moinard *et al.* [97] have used TV inpainting to predict DCT coefficients in a JPEG-based codec.

## 2.7 Modifications, Extensions, and Applications

A progressive mode option is a useful feature of a codec. It allows to encode and transmit data in a coarse-to-fine way. Thus, in the decoding phase, the representation can be subsequently refined while reading the data stream. In [117], two progressive modes have been suggested for the EED-based codec, and it has been shown that for high compression rates, their quality is competitive to JPEG and JPEG 2000.

By construction, PDE-based codecs are well-suited for encoding specific regions of interest with higher precision. All one has to do is to increase the density of the inpainting data in the region of interest. For more details, we refer to [106].

Since a large fraction of modern imagery consists of colour image data, codecs should be able to handle colour images efficiently. While for most PDE approaches, extensions to vector- and even matrix-valued data exist, these modifications are not necessarily optimal for compression applications. As a remedy, in [107] an extension of the EED-based codec to colour images is proposed that uses the YCbCr representation. The perceptually relevant luma channel is stored with fairly high accuracy, while the chroma channels are encoded with very sparse data. In the reconstruction phase the chroma inpainting is guided by the structural information from the luma channel.

Extending PDE-based codecs from 2-D images to three-dimensional data sets does not create severe difficulties. Most PDE's have natural extensions to higher dimensions, and also other concepts generalise in a natural way: For instance a rectangular subdivision in 2D is replaced by a cuboidal subdivision in 3D [118]. Because of the richer neighbourhood structure, the redundancy in higher dimensional data allows to achieve a higher compression rate for the same quality as a lower dimensional codec.

PDE-based compression strategies have also been investigated for encoding contours [118] and surfaces [6, 113]. These publications follow the philosophy of PDE-based image compression, but replace the Laplacian by the contour curvature or the Laplace–Beltrami operator.

Obviously one can apply any method for compressing 3D data also to video coding, if one models a video or parts of it as a spatiotemporal data block. Other video coding approaches have been suggested that use inpainting concepts within the H.264/MPEG-4 AVC video coding standard [41, 86, 97]. In [119], the authors have implemented a video compression system that combines PDE-based image compression with pose tracking.

Cryptographic applications are studied in [92], where the authors combine PDE-based compression with steganographic concepts in order to hide one image in another one, or parts of an image in other parts.

## 2.8 Relations to Other Methods

PDE-based codecs that select the inpainting mask with triangular or rectangular subdivisions have structural similarities to piecewise polynomial image approximations based on adaptive triangulations or quadtrees. Extensive research has been performed on these approximations; see [13, 30, 35, 40, 44, 75, 77, 82, 83, 122, 124, 125] and the references therein. Often such approaches use linear polynomials within each triangle or rectangle. In this case, one may also interpret them as a solution of the Laplace equation with Dirichlet boundary data obtained from a linear interpolation of the vertex data. Thus, they can be seen as specific localised PDE-based codecs. Alternative interpretations can be given in terms of finite element approximations. In the one-dimensional case, the linear spline approximation is even fully equivalent to homogeneous diffusion inpainting.

Inpainting with linear differential operators allows also an analytical representation of its solution in terms of the Green's function of the operator. This has been used in [66] to relate linear PDE-based inpainting to sparsity concepts: Discrete Green's functions serve as atoms in a dictionary that gives a sparse representation of the inpainting solution. In the one-dimensional case, discrete analytic derivations are presented in [110].

On the other hand, continuous Green's functions are also used as radial basis functions in scattered data interpolation [20]. Moreover, some radial basis functions can be seen as rotationally invariant multidimensional extensions of spline interpolation. This establishes a connection between PDE-based inpainting and image representations in terms of radial basis functions and splines, such as [4, 38, 49, 129].

## 3 Inpainting with Homogeneous Diffusion

In this section, we will briefly present the homogeneous diffusion reconstruction method (also known as Laplace interpolation) that lies at the basis of our approach and will be used for most of the results presented here. Homogeneous diffusion is among the simplest inpainting processes that one can consider. This makes it suitable for theoretical investigations. Nevertheless, one should emphasise that even such a simple method can yield very good results if the interpolation data is chosen in an appropriate way; see e.g. [8, 63, 91, 101].

Let  $f : \Omega \rightarrow \mathbb{R}$  be a smooth function on some bounded domain  $\Omega \subset \mathbb{R}^n$  with a sufficiently regular boundary  $\partial\Omega$ . Throughout this work, we will restrict ourselves to the case  $n = 1$  (1D signals) and  $n = 2$  (greyscale images), although many results will also be valid for arbitrary  $n \geq 1$ . Moreover, let us assume that there exists a set of known data  $\Omega_K \subsetneq \Omega$ . Homogeneous diffusion

inpainting considers the following partial differential equation with mixed boundary conditions.

$$\Delta u = 0 \quad \text{on } \Omega \setminus \Omega_K, \quad (1)$$

$$u = f \quad \text{on } \Omega_K, \quad (2)$$

$$\partial_n u = 0 \quad \text{on } \partial\Omega \setminus \partial\Omega_K, \quad (3)$$

where  $\partial_n u$  denotes the derivative of  $u$  in outer normal direction. We assume that both boundary sets  $\partial\Omega_K$  and  $\partial\Omega \setminus \partial\Omega_K$  are non-empty. Equations of this type are commonly referred to as mixed boundary value problems and sometimes also as Zaremba's problem named after Stanislaw Zaremba, who studied such equations already in 1910 [141]. The existence and uniqueness of solutions has been extensively analysed during the last century. Showing that (1)–(3) is indeed solvable is by no means trivial. Generally, one can either show the existence of solutions in very weak settings or one has to impose strong regularity conditions on the domain. The references [5, 96] discuss the solvability in a general way. In [95] it is shown that a Hölder continuous solution exists if the data is sufficiently regular. In [19], the author discusses the regularity of solutions on Lipschitz domains. A more general existence theory for solutions is given in [50]. Further investigations on mixed boundary value problems can also be found in [56, 81]. A particularly easy case is the 1D setting, where the solution can obviously be expressed using piecewise linear splines interpolating data on  $\partial\Omega_K$ .

For convenience we introduce the confidence function  $c$  which states whether a point is known or not:

$$c(x) := \begin{cases} 1 & \text{for } x \in \Omega_K, \\ 0 & \text{for } x \in \Omega \setminus \Omega_K. \end{cases} \quad (4)$$

Then it is possible to write (1)–(3) as

$$c(x) (u(x) - f(x)) - (1 - c(x)) \Delta u(x) = 0 \quad \text{on } \Omega, \quad (5)$$

$$\partial_n u = 0 \quad \text{on } \partial\Omega \setminus \partial\Omega_K. \quad (6)$$

For most parts of this text we will prefer this formulation, as it is more comfortable to work with in the discrete setting, which can be obtained as follows. Let  $J := \{1, \dots, N\}$  be the set of indices enumerating the discrete sample positions, and  $K \subseteq J$  the subset of indices of known samples. Then we can express the discrete version of  $f$  as a vector  $\mathbf{f} = (f_1, \dots, f_N)^\top$  and the corresponding solution as a vector  $\mathbf{u} \in \mathbb{R}^N$ . The binary mask  $\mathbf{c} \in \mathbb{R}^N$ , where  $c_i := 1$  if  $i \in K$  and  $c_i := 0$  otherwise, indicates the positions of the Dirichlet boundary data. At last, the Laplacian  $\Delta$  is discretised by standard means of finite differences [98]. Hence, a straightforward discretisation of (5)–(6) on a regular grid yields

$$\mathbf{C}(\mathbf{u} - \mathbf{f}) - (\mathbf{I} - \mathbf{C})\mathbf{A}\mathbf{u} = \mathbf{0} \quad (7)$$

where  $\mathbf{I}$  is the identity matrix,  $\mathbf{C} := \text{diag}(\mathbf{c})$  is a diagonal matrix with the components of  $\mathbf{c}$  as its entries, and  $\mathbf{A} = (a_{i,j})$  is a symmetric  $N \times N$  matrix, describing the discrete Laplace operator  $\Delta$  with homogeneous Neumann boundary conditions on  $\partial\Omega \setminus \partial\Omega_K$ . Its entries are given by

$$a_{i,j} = \begin{cases} \frac{1}{h_\ell^2} & (j \in \mathcal{N}_\ell(i)), \\ - \sum_{\ell \in \{x,y\}} \sum_{j \in \mathcal{N}_\ell(i)} \frac{1}{h_\ell^2} & (j = i), \\ 0 & (\text{else}), \end{cases} \quad (8)$$

where  $\mathcal{N}_\ell(i)$  are the neighbours of pixel  $i$  in  $\ell$ -direction, and  $h_\ell$  is the corresponding grid size. By a simple reordering of the terms, (7) can be rewritten as the following linear system:

$$\underbrace{(\mathbf{C} - (\mathbf{I} - \mathbf{C}) \mathbf{A})}_{=: \mathbf{M}} \mathbf{u} = \mathbf{C} \mathbf{f}. \quad (9)$$

It has been shown in [90] that this linear system of equations has a unique solution and that it can be solved efficiently with bidirectional multigrid methods.

## 4 Optimisation Strategies in 1D

The choice of the position of the Dirichlet boundary data has a strong influence on the quality of the reconstruction. In order to gain some analytical insight on this problem, we restrict ourselves in this section to the 1D continuous setting and consider in Section 4.1 how to find the optimal positions of the mask points  $\mathbf{c}$ . Optimising position and value of the Dirichlet data simultaneously will be treated in Section 4.2.

### 4.1 Optimal Knots for Interpolating Convex Functions

In this section, we assume that  $f : [a, b] \rightarrow \mathbb{R}$  is always a strictly convex and continuously differentiable function. Our goal is to find a distribution of  $N + 1$  knot sites  $\{c_i\}_{i=0}^N$  in the interval  $[a, b]$  such that the interpolation error with piecewise linear splines becomes minimal in the  $L_1$  norm. For 1D formulations, this is equivalent to determining the Dirichlet boundary data in (1)–(3) such that the solution  $u$  gives the best possible reconstruction to  $f$  in the  $L_1$  sense. In concrete terms, this means that we seek  $N + 1$  positions inside the interval  $[a, b]$  with

$$a =: c_0 < c_1 < c_2 < \dots < c_{N-1} < c_N := b \quad (10)$$

and a piecewise linear spline  $L(x; \{c_i\}_{i=0}^N)$  interpolating  $f$  at the positions  $c_i$ , such that the error

$$E(\{c_i\}_{i=0}^N) := \int_a^b |L(x; \{c_i\}_{i=0}^N) - f(x)| dx \quad (11)$$

becomes minimal. This optimisation problem is also called *free knot problem* and has been studied for more than fifty years. We refer to [61, 76] for similar considerations as in our work and to [11, 37, 39, 73] and the references therein for more general approaches. Note that it is quite common to relax the interpolation condition and to generalise the problem to explicitly allow approximating functions. Further details on interpolation and approximation techniques can be found in [112]. Alternative ways to optimise linear spline interpolation are discussed e.g. in [10].

For technical reasons, the knots  $c_0$  and  $c_N$  in (10) are fixed at the boundary of the considered interval. The choice of the  $L_1$  norm is especially attractive in this case: Due to the convexity of  $f$ , the integrand

$$L(x; \{c_i\}_{i=0}^N) - f(x)$$

is nonnegative for all  $x$  in  $[a, b]$ . Thus, we can simply omit the absolute value in (11). This observation simplifies the derivation of optimality conditions below. Furthermore, the requirement that the linear spline  $L$  must coincide with  $f$  at the knot sites  $c_i$  allows us to state the interpolating function in an analytic form: If  $x \in [c_i, c_{i+1}]$ , then

$$L(x; \{c_i\}_{i=0}^N) = \frac{f(c_{i+1}) - f(c_i)}{c_{i+1} - c_i}(x - c_i) + f(c_i). \quad (12)$$

Note that requiring that the  $c_i$  are distinct is necessary to avoid a division by 0. A straightforward computation gives

$$\begin{aligned} E(\{c_i\}_{i=0}^N) &= \int_a^b (L(x; \{c_i\}_{i=0}^N) - f(x)) dx \\ &= \frac{1}{2} \sum_{i=0}^{N-1} (c_{i+1} - c_i) (f(c_{i+1}) + f(c_i)) \\ &\quad - \int_a^b f(x) dx. \end{aligned} \quad (13)$$

This expression also corresponds to the error of the composite trapezoidal rule for the numerical integration of  $f$  with non-equidistant integration intervals.

Equation (13) will be our starting point for developing an algorithm to determine the optimal knot sites. However, before we will do so, we present a result which shows the difficulty of the free knot optimisation problem.

**Proposition 1.** *If the function  $f : [a, b] \rightarrow \mathbb{R}$  is strictly convex and twice continuously differentiable, then the energy (11) is convex in  $\{c_i\}_{i=0}^N$  for 3 knots (i.e.  $N = 2$ ). In general, it is not convex for any other number of knots larger than 3 (i.e.  $N > 2$ ).*

*Proof.* In the case of three knots, we only have one free variable, and it follows from (13) that the error is given by

$$E(c_1) = \frac{1}{2} \left( (c_1 - a) (f(a) + f(c_1)) + (b - c_1) (f(b) + f(c_1)) \right) - \int_a^b f(x) dx. \quad (14)$$

Further, the second derivative of  $E$  is given by

$$\frac{\partial^2}{\partial c_1^2} E(c_1) = \frac{b-a}{2} \frac{\partial^2}{\partial c_1^2} f(c_1) > 0 \quad \forall c_1 \in [a, b]. \quad (15)$$

In order to demonstrate that the error function is nonconvex for a higher number of interpolation points, it suffices to provide a counterexample. Let us consider the function  $f(x) = \exp(x)$  on the interval  $[-15, 15]$  as well as the two knot sets  $U_1 = \{-15, 10.65, 14.65, 15\}$  and  $U_2 = \{-15, -1.2, 12.5, 15\}$ . If  $E$  were convex, then it must also be convex along the line in  $\mathbb{R}^4$  that connects  $U_1$  and  $U_2$  (interpreting both knot sets as vectors in  $\mathbb{R}^4$ ). However, the plot of  $E((1-t)U_1 + tU_2)$  with  $t \in [0, 1]$  depicted in Fig. 1 displays a nonconvex behaviour.  $\square$

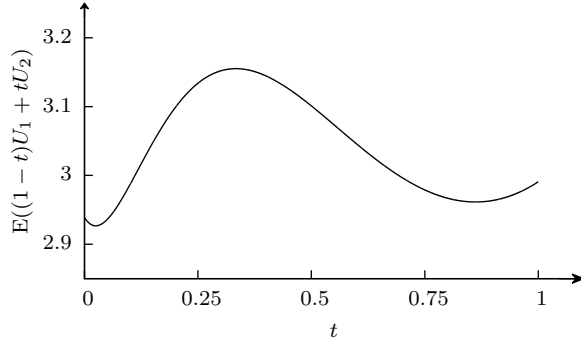


**Fig. 1.** Evolution of the error for interpolating the function  $\exp(x)$  with knots along the segment with bounds  $U_1 = (-15, 10.65, 14.65, 15)^\top$  and  $U_2 = (-15, -1.2, 12.5, 15)^\top$ . It shows a nonconvex behaviour. For better readability, the function values have been rescaled by a factor  $10^{-6}$ .

We remark that the previous proposition does not claim that the energy can never be convex for more than three knots. Indeed, for affine functions of the form  $mx + k$  with real coefficients  $m$  and  $k$  the energy is identical 0 for any number of knots, and thus also convex. This shows that even under weaker conditions as in the proposition, the energy may be convex.

**A New Algorithm for the Free Knot Problem for Linear Spline Interpolation** A necessary condition for a minimiser  $\{c_i^*\}_{i=0}^N$  of (13) is  $\nabla E(\{c_i^*\}_{i=0}^N) = 0$ . However, it follows from Proposition 1 that this condition is not sufficient. There may exist several global and/or local minima. A simple computation leads to the following system of  $N - 1$  nonlinear equations in the  $N - 1$  unknowns  $c_1, \dots, c_{N-1}$ :

$$f'(c_i) = \frac{f(c_{i+1}) - f(c_{i-1})}{c_{i+1} - c_{i-1}}, \quad i = 1, \dots, N - 1. \quad (16)$$

It should be noted that each knot only depends on its direct neighbours. Therefore, odd indexed knots only depend on even indexed knots and vice versa. Since  $f$  is strictly convex, it follows that  $f'$  is strictly monotonically increasing. Thus, its inverse exists and is unique at every point of the considered interval. This motivates the following iterative scheme.

---

**Algorithm 1: Spatial Optimisation in 1D**

---

***Input:***

$N + 1$ , the desired number of knots.

***Initialisation:***

Choose any initial distribution  $\{c_i^0\}_{i=0}^N$  with  $c_0^0 = a$  and  $c_N^0 = b$ , e.g. a uniform distribution of the knots on the interval  $[a, b]$ .

***Repeat until a fixed point is reached:***

**Update even knots for all possible  $i$ :**

$$c_{2i}^{k+1} := (f')^{-1} \left( \frac{f(c_{2i+1}^k) - f(c_{2i-1}^k)}{c_{2i+1}^k - c_{2i-1}^k} \right). \quad (17)$$

**Update odd knots for all possible  $i$ :**

$$c_{2i+1}^{k+1} := (f')^{-1} \left( \frac{f(c_{2i+2}^{k+1}) - f(c_{2i}^{k+1})}{c_{2i+2}^{k+1} - c_{2i}^{k+1}} \right). \quad (18)$$

***Output:***

The final knot distribution  $\{c_i^*\}_{i=0}^N$ .

---

Observe that the above scheme is similar to a Red-Black Gauß–Seidel scheme for the solution of linear systems: We update the variables iteratively and use newly gained information as soon as it becomes available without interfering with the direct neighbours of the data point. An important issue is that the knots  $c_i$  are not allowed to fall together. The following proposition shows that this cannot happen.



**Proposition 2.** *The iterative scheme (17)–(18) preserves the ordering of the knot positions. Thus, we have e.g.*

$$c_{i-1}^k < c_i^k < c_{i+1}^k \Rightarrow c_{i-1}^{k+1} < c_i^{k+1} < c_{i+1}^{k+1} \quad \forall k, i. \quad (19)$$

*Proof.* Since  $f$  is differentiable on  $[c_{i-1}, c_{i+1}]$  for all  $i$ , the mean value theorem guarantees the existence of a  $c_i$  in  $(c_{i-1}, c_{i+1})$  such that

$$f'(c_i) = \frac{f(c_{i+1}) - f(c_{i-1})}{c_{i+1} - c_{i-1}}. \quad (20)$$

Thus, our iterative scheme must necessarily preserve the order of the knots.  $\square$

The next theorem shows that the iterates from our algorithm monotonically decrease the considered energy.

**Theorem 1.** *If the function  $f : [a, b] \rightarrow \mathbb{R}$  is strictly convex and twice continuously differentiable, the iterates  $\left(\{c_i^k\}_{i=0}^N\right)_k$  obtained in (17) and (18) decrease the  $L_1$  error (11) in each step, i.e. we have*

$$E\left(\{c_i^{k+1}\}_{i=0}^N\right) \leq E\left(\{c_i^k\}_{i=0}^N\right) \quad \forall k. \quad (21)$$

*Proof.* By alternating between the update of the odd and even indexed sites, the problem decouples. The new value of  $c_i^{k+1}$  only depends on  $c_{i-1}^k$  and  $c_{i+1}^k$ , which are fixed. Therefore, the problem is localised, and we can update all the even/odd indexed knots independently of each other. It follows that one iteration step is equivalent to finding the optimal  $c_i^{k+1}$  such that the interpolation error becomes minimal on  $[c_{i-1}^k, c_{i+1}^k]$  for all even/odd  $i$ . The global error can now be written as the sum of all the errors over the intervals  $[c_{i-1}^k, c_{i+1}^k]$  and will necessarily decrease when each term of this sum decreases. Proposition 1 shows that the considered energy is convex for three knots. Thus,  $\nabla E(\{c_j^k\}_{j=i-1}^{i+1}) = 0$  is not only a necessary, but also a sufficient condition for being a minimum on  $[c_{i-1}^k, c_{i+1}^k]$ . This means that (17) will not increase the error when updating even indexed knots and subsequently, (18) will not increase the error while updating the odd numbered sites. Therefore, it follows that the overall error cannot increase in an iteration step.  $\square$

Since the error is bounded from below by 0, we also obtain the following result.

**Corollary 1.** *The sequence  $\left(E\left(\{c_i^k\}_{i=0}^N\right)\right)_k$  is convergent.*

Note that the previous statements do not claim the convergence of the sequence  $\left(\{c_i^k\}_{i=0}^N\right)_k$ . Since the problem is nonconvex, the global minimum of the considered energy is not necessarily unique. In that case, our algorithm might alternate between several of the minimisers. These minimisers are,

from a qualitative point of view, all equivalent, since they yield the same error. However, they might not be the global minimiser. Also note that the theorem of Bolzano-Weierstrass asserts that  $(\{c_i^k\}_{i=0}^N)_k$  contains at least one convergent subsequence since all the  $c_i^k$  must necessarily lie in the interval  $[a, b]$ . Finally, we remark that in our test cases the results were always of very good quality. This gives rise to the conjecture that the found knot distributions are close to a global minimum.

**Numerical Experiments** Let us now perform experiments with our new algorithm. We consider the convex function

$$f(x) = \exp(2x - 3) + x$$

on the interval  $[-4, 4]$ . Figure 2 depicts the evolution of the error, while Fig. 3 exhibits the resulting distribution of the knots. The experiments were done with a randomised initial distribution of the knots and 5000 iterations. Interestingly, the iterates always converged already after very few iterations. In accordance with the theory from the previous section, we also note that the error is monotonically decreasing, both with respect to the number of knots and with respect to the number of iterations. Another interesting observation is the influence of an additionally introduced knot on the other knots: Adding further interpolation sites has a global influence on all the other knots. Moreover, we encounter a higher knot density in regions with large curvature than in flat regions. This is in agreement with the theory of Belhachmi *et al.* [8].

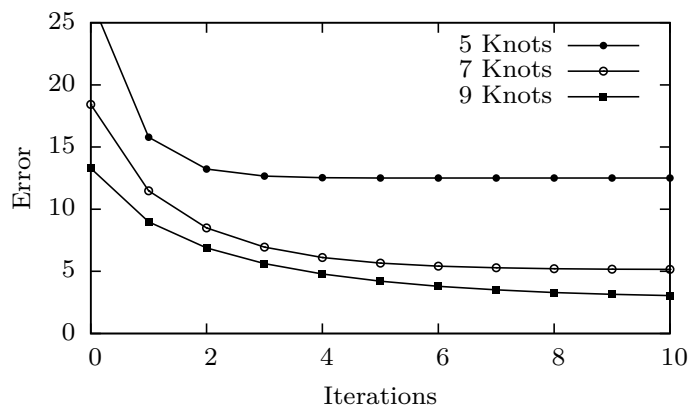


**Fig. 2.** Evolution of the  $L_1$  error as a function of the iterates for different numbers of knots for the function  $f(x) = \exp(2x - 3) + x$  on the interval  $[-4, 4]$ . Note that the error is decreasing both with respect to the number of knots and with respect to the number of iterations. Furthermore, the curves suggest a rather fast convergence to a stationary energy value.

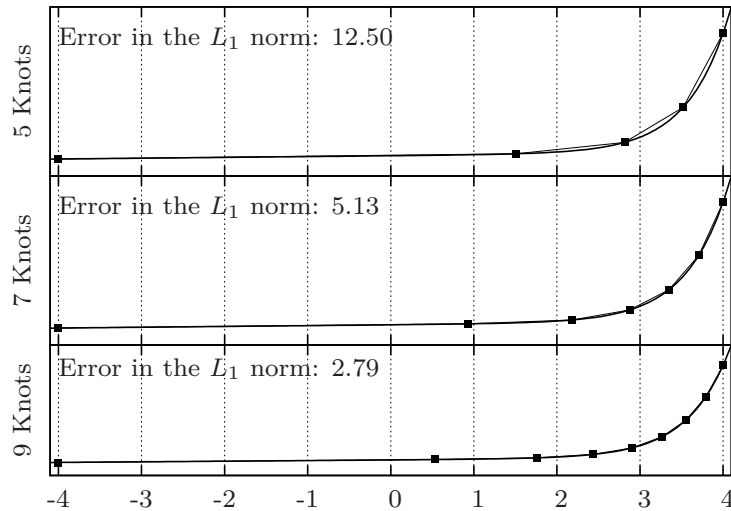


**Fig. 3.** Distribution of the knots corresponding to Figure 2 for the converged state of the function  $f(x) = \exp(2x - 3) + x$ . Note that there are almost no knots in flat regions, whereas there is a high density in regions with large curvature. Changing the number of knots actually influences the position of all the knots.

## 4.2 Optimal Knots for Approximating Convex Functions

In the previous section, we have seen how to optimise the *location* of the interpolation data. A next step would be to investigate how much an optimisation of the *grey value data* at these sites could further improve the result. To do so, we no longer require that the function value and the value of the interpolant must coincide at the knot locations. Instead, we consider an approximation problem and require that the overall reconstruction minimises the  $L_1$  error on the considered domain. As in the previous section, we again use piecewise linear splines. Such approximations by means of first degree splines have a long history, and there exist results for many special cases. In [123], the best approximation of strictly convex functions in the least squares sense has been analysed, while [34] cites general conditions for the determination of best approximations of strictly convex functions in the  $L_\infty$  sense. Theoretical results can also be found in [73]. In [100], it is shown that an optimal approximation of convex functions with splines is not necessarily unique, a problem which we already mentioned in the stricter case of convex spline interpolation. Finally, [31, 109] supply algorithms for determining such approximations.

In order to minimise the  $L_1$  error between a strictly convex function  $f : [a, b] \rightarrow \mathbb{R}$  and a piecewise linear spline in an approximation setting, we use an algorithm by Hamideh [61]. It relies on a classical result from approximation theory:

**Theorem 2.** For any function  $f \in C([a, b])$ , which is strictly convex in  $[a, b]$ , the optimal straight line approximation to  $f$  in the  $L_1$  sense on  $[a, b]$  interpolates the function at the points

$$\xi_1 := \frac{3}{4}a + \frac{1}{4}b \quad \text{and} \quad \xi_2 := \frac{1}{4}a + \frac{3}{4}b. \quad (22)$$

*Proof.* This result can be verified by direct computation. Alternatively, a detailed proof can also be found in [112].  $\square$

This gives rise to the following algorithm.

---

**Algorithm 2: Optimal Approximation in 1D**

---

**Input:**

$N + 1$  the number of desired knots.

**Initialisation:**

Choose an arbitrary distribution of  $N + 1$  knots with  $c_0 := a$  and  $c_N := b$ .

**Compute:**

Repeat these steps until a fixed point is reached.

1. On each subinterval  $[c_{i-1}, c_i]$ , define the points

$$\xi_{i,1} := \frac{3c_{i-1} + c_i}{4}, \quad \xi_{i,2} := \frac{c_{i-1} + 3c_i}{4} \quad (23)$$

as well as the corresponding line  $\ell_{i-1}$  passing through these points:

$$\ell_{i-1}(x) := \frac{f(\xi_{i,2}) - f(\xi_{i,1})}{\xi_{i,2} - \xi_{i,1}}(x - \xi_{i,1}) + f(\xi_{i,1}) \quad (24)$$

2. Determine for all  $i$  the new knot position  $c_i$  by intersecting the lines  $\ell_{i-1}$  and  $\ell_i$ , e.g. solve

$$\ell_{i-1}(c_i) = \ell_i(c_i) \quad (25)$$

for  $c_i$ .

**Output:**

The final knot distribution  $\{c_i\}_{i=0}^N$ .

---

The algorithm of Hamideh is similar to our Algorithm 1 for interpolation: Both use iteratively locally optimal solutions to perform a global optimisation. In addition, the following properties are shown in [61]:

1. The resulting sequence of  $L_1$  errors  $\left(E(\{c_i^k\}_{i=0}^N)\right)_k$  is convergent.
2. For all  $i = 1, \dots, N - 1$ , it holds that

$$\liminf_{k \rightarrow \infty} |c_{i+1}^k - c_i^k| > 0, \quad (26a)$$

$$\lim_{k \rightarrow \infty} |c_i^{k+1} - c_i^k| = 0, \quad (26b)$$

where  $\left(\{c_i^k\}_{i=0}^N\right)_k$  is our sequence of knot sets. Thus, two distinct knots cannot fall together.

3. If the unknown optimal spline fulfils certain continuity conditions, one can guarantee that the above algorithm converges towards an optimal solution.

Further analytic results on the optimal knot distribution can also be found in [76].

**Numerical Experiments** We investigate the knot distribution for different number of knots and repeat the experiments of Section 4.1 using now the algorithm of Hamideh. Our main interest lies in the performance of a combined optimisation over a sequential optimisation of the position and the corresponding value of the interpolation data. To this end, we also consider a tonal optimisation that adjusts the function values for our free knot result. This additional task is carried out as a postprocessing step. Since the position of the mask values is optimised in an  $L_1$  setting, we use the same framework for the tonal optimisation, too. Due to the fact that for a fixed set of knots, we can express our interpolating spline as a linear combination of first degree B-Splines, we can express the tonal optimisation as a linear regression task with respect to the  $L_1$  norm. It is well-known that such problems can be reduced to linear programs which can efficiently be solved by standard solvers from the literature. Our findings are summarised in Tab. 1, and a visual comparison between the obtained mask sets for a set of seven knots is given in Fig. 4.

**Table 1.** Error measures for our interpolation algorithm and the approximation algorithm of Hamideh for different numbers of mask points applied to the function  $x \mapsto \exp(2x - 3) + x$  on the interval  $[-4, 4]$ . For our method we list the error without additional tonal optimisation and with additional tonal optimisation.

$N + 1$	Our method		Hamideh
	no tonal optim.	with tonal optim.	
5	12.501	4.229	3.982
7	5.134	1.810	1.748
9	2.785	0.999	0.977

Although the knot distribution in Fig. 4 for the approach of Hamideh is similar to the one found with interpolation, the corresponding errors in Tab. 1 are significantly lower, since the reconstruction can adapt much better to the original function when compared to the interpolation framework. Nevertheless, we also observe a substantial gain of the tonal optimisation. Even though we cannot outperform the combined optimisation, we achieve competitive results, in particular for larger values of  $N$ .

Our investigations in the 1D case show that a careful optimisation of the positions (spatial information) and greyvalues (tonal information) of

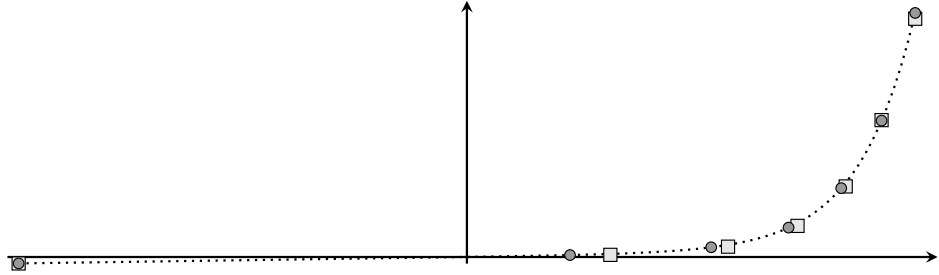


**Fig. 4.** Comparison between the knots found with our method (dark grey disks) and the method of Hamideh (light grey squares) for the function  $\exp(2x - 3) + x$  along the interval  $[-4, 4]$  (dotted line).

the data can lead to significant improvements compared to a purely spatial tuning. Moreover, a sequential optimisation is almost as good as a combined optimisation of the data. The next step in our strategy will be to adapt these ideas to the two-dimensional setting such that we can efficiently apply them on discrete image data.

## 5 Optimisation Strategies in 2D

Unfortunately, our interpolation algorithm from Section 4 can hardly be used directly on 2D image data. First of all, we would be restricted to convex/concave images. Of course, one could always segment an arbitrary image into convex and concave regions and treat them separately, but in many cases this would lead to heavily oversegmented images and a suboptimal global distribution of the data points for the reconstruction. Secondly, the solution of (5)–(6) in higher dimensions cannot be written in terms of simple piecewise linear interpolation: To characterise it analytically would require more complicated expressions that involve Green’s functions [66]. Therefore, we want to consider other approaches here. Nevertheless, they exploit the basic ideas and findings of a spatial and tonal optimisation from the previous section.

For practical reasons, we present a two-step optimisation strategy: First we consider an interpolation approach to optimise the spatial data. Afterwards we optimise the tonal information at the points obtained in the first step. This strategy can be justified by the fact that in the 1D case, the obtained knot distributions for the interpolation and approximation algorithms were similar. For the optimisation of the data sites we investigate two methods: An analytic approach proposed in [8] that exploits the theory of shape optimisation, and our probabilistic sparsification approach from [91]. Finally we complement our pure interpolation framework with a best approximation scheme that incorporates tonal optimisation in our model.

## 5.1 Optimising Spatial Data

**Analytic Approach** In order to approach the question about the optimal data selection, Belhachmi *et al.* [8] use the mathematical theory of shape optimisation. This theory optimises topological properties of given objects. Belhachmi *et al.* seek the optimal shape of the set of Dirichlet boundary data in (1)–(3). They show that the density of the data points should be chosen as an increasing function of the Laplacian magnitude of the original image. However, this optimality result returns a continuous density function rather than a discrete pixel mask. This yields an additional problem that is also discussed in [8], namely, how to obtain the best discrete (binary) approximation to a continuous density function. Belhachmi *et al.* suggest the following strategy to obtain a point mask based upon  $|\Delta f|$ . First one applies a small amount of Gaussian presmoothing with standard deviation  $\sigma$  to obtain  $f_\sigma$ . This is a common procedure in image analysis to ensure the differentiability of the data. Then one computes the Laplacian magnitude  $|\Delta f_\sigma|$  and rescales it such that its mean represents the desired point density given as fraction  $d$  of all pixels. Finally any dithering algorithm that preserves the average grey value can be applied to obtain the binary point mask.

In [8] the classical error diffusion method of Floyd and Steinberg [51] is used. However, we favour the more sophisticated electrostatic halftoning [116] over simpler dithering approaches, since it has proven to yield very good results for discretising a continuous distribution function. Figure 5 shows the superiority of electrostatic halftoning over Floyd-Steinberg dithering in terms of the mean squared error (MSE)

$$\text{MSE}(\mathbf{u}, \mathbf{f}) = \frac{1}{|J|} \sum_{i \in J} (f_i - u_i)^2, \quad (27)$$

where  $\mathbf{u}$  denotes the reconstruction,  $\mathbf{f}$  the original image and  $J$  the set of all pixel indices. Since any dithering method introduces errors, it remains an open question if this is the most suitable approach to discretise the continuous optimality result.

The theory of Belhachmi *et al.* [8] demands the data points to be chosen as an increasing function of  $|\Delta f|$ . However, the optimal increasing function depends on the details of the underlying model. One option is to use the identity function of the Laplacian magnitude, as was done in [91]. In the present work, we introduce an additional parameter  $s > 0$  and dither  $|\Delta f_\sigma|^s$  instead. This choice can also be motivated from the original paper [8] and allows to tune the density of the selected points in homogeneous regions. The complete method, which we call the analytic approach, is summarised below.

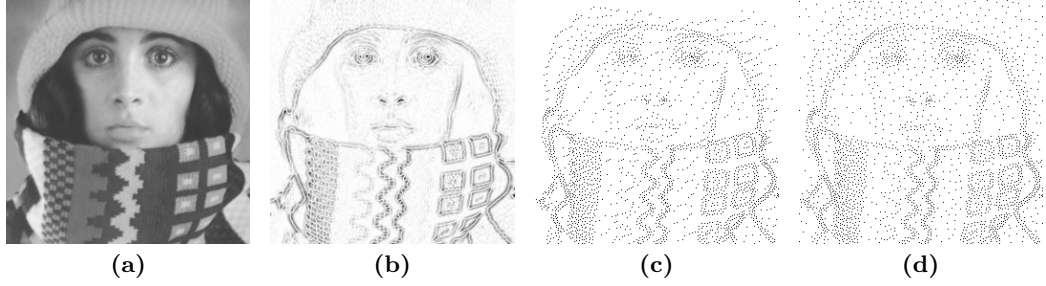


**Fig. 5.** (a) Original test image *trui* ( $256 \times 256$  pixels). (b) Smoothed Laplacian magnitude of (a) using  $\sigma = 1$  (rescaled and inverted). (c, d) Dithered versions of (b) using Floyd-Steinberg error diffusion and electrostatic halftoning, respectively. With (c) and (d) as mask for homogeneous diffusion inpainting we obtain an MSE of 138.98 and 101.14, respectively. All the images use floating point values in the range from 0 to 255 for the pixels. The discrete masks have a density of 4%.

---

### Algorithm 3: Analytic Approach

---

**Input:**

Original image  $f$ , Gaussian standard deviation  $\sigma$ , exponent  $s$ , desired pixel density  $d$ .

**Compute:**

1. Perform Gaussian presmoothing with standard deviation  $\sigma$ :  $f_\sigma = K_\sigma * f$ .
2. Compute  $|\Delta f_\sigma|^s$ .
3. Rescale  $|\Delta f_\sigma|^s$  to

$$\frac{d \cdot f_{\max}}{\text{mean}(|\Delta f_\sigma|^s)} \cdot |\Delta f_\sigma|^s$$

where  $f_{\max}$  is the maximal possible grey value.

4. Apply electrostatic halftoning to obtain  $c$ .

**Output:**

Discrete pixel mask  $c$ .

---

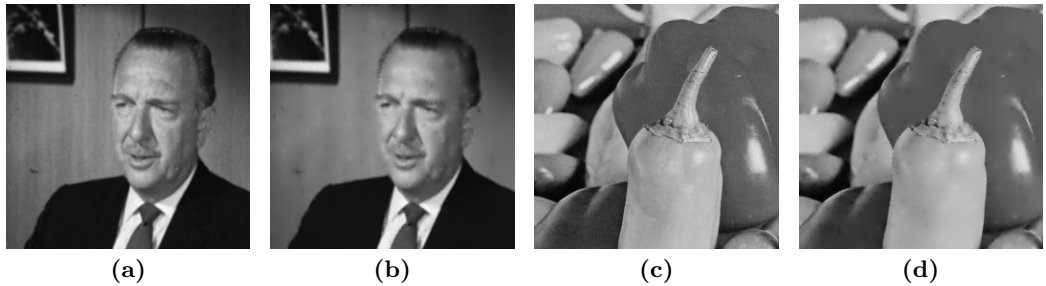


**Fig. 6.** (a, c) Original test images *walter* ( $256 \times 256$  pixels) and *peppers* ( $256 \times 256$  pixels). (b, d) Best reconstruction results with 4% of all pixels, using probabilistic sparsification, nonlocal pixel exchange and grey value optimisation. The image (b) has an MSE of 12.45, while image (d) has an MSE of 25.10.

In order to evaluate the analytic approach, let us apply it on the test image *trui* (see Fig. 5(a)). We aim at a mask pixel density of 4% ( $d = 0.04$ )



of all pixels. The parameters  $\sigma$  and  $s$  are chosen such that the MSE of the reconstruction becomes minimal. This was achieved with  $\sigma = 1.6$  and  $s = 0.8$ . For comparison, we also consider two masks with the same amount of pixels: a mask with points on a regular grid and a randomly sampled mask. Figure 8 shows these two masks and the one created with the analytic approach in the first column as well as the corresponding reconstructions in the second column. We observe that the reconstruction quality highly benefits from a dedicated point selection. These results are confirmed by the Columns 3, 4 and 5 of Tab. 4, which depicts quantitative results for several test images from Fig. 5(a), Fig. 6(a), and Fig. 6(c).

As already mentioned, the analytic approach is real-time capable if a fast dithering method is used. However, rather than on speed, the focus of our present work is to maximise the quality of the reconstruction. Therefore, in the next subsection we present an alternative algorithm that is slower but outperforms the analytic approach in terms of quality.

**Probabilistic Sparsification** We have seen that the analytic approach offers a clean strategy how to choose optimal spatial data in a continuous image. However, due to certain degrees of freedom in the modelling, errors caused by the dithering algorithm, and discretisation effects, its results on digital images cannot be optimal. As an alternative, we consider now a discretise-then-optimize strategy. This way we can directly search for a binary-valued mask  $\mathbf{c}$  by working with the discrete inpainting formulation from (7). An immediate consequence of this approach is that there are only finitely many combinations for  $\mathbf{c}$ . Unfortunately, already for an image of size  $256 \times 256$  pixels and a desired pixel density of 4% there are  $\binom{65536}{2621} \approx 2 \cdot 10^{4777}$  possible masks. To tackle this combinatorial problem we suggest a method called probabilistic sparsification. It uses a greedy strategy to reduce the search space.

Let  $\mathbf{f}$  be a given discrete image and let  $\mathbf{r}(\mathbf{c}, \mathbf{f})$  be the function that computes the solution  $\mathbf{u}$  of the discrete homogeneous inpainting process (9) with a mask  $\mathbf{c}$ :

$$\mathbf{r}(\mathbf{c}, \mathbf{f}) := \mathbf{u} = (\mathbf{C} - (\mathbf{I} - \mathbf{C})\mathbf{A})^{-1} \mathbf{C}\mathbf{f}. \quad (28)$$

The goal is to find the pixel mask  $\mathbf{c}$  that selects a given fraction  $d$  of all pixels and minimises  $\text{MSE}(\mathbf{u}, \mathbf{f})$ .

Starting with a full mask, where every pixel is chosen, probabilistic sparsification iteratively removes the least significant mask pixels until a desired density is reached. More specifically, we randomly choose a fraction  $p$  of candidate pixels from the current mask. These pixels are removed from the mask, and an inpainting reconstruction is calculated. The significance of a candidate pixel can then be estimated by computing the local error, i.e. the squared grey value difference of the inpainted and original image in this pixel.

Then we permanently remove the fraction  $q$  of the candidates that exhibit the smallest local error from the mask, and we insert back again the remaining fraction  $(1 - q)$  of the candidates. A detailed description of our algorithm is given below.

---

**Algorithm 4: Stochastic Sparsification**

---

**Input:**

Original image  $\mathbf{f}$ , fraction  $p$  of mask pixels used as candidates, fraction  $q$  of candidate pixels that are removed in each iteration, desired pixel density  $d$ .

**Initialisation:**

$\mathbf{C} := \text{diag}(1, \dots, 1)^\top$  and  $K := J$ .

**Compute:**

Do

1. Choose randomly a candidate set  $T$  of  $p \cdot |K|$  pixel indices from  $K$ .
2. For all  $i \in T$  set  $c_i := 0$ .
3. Compute  $\mathbf{u} := \mathbf{r}(\mathbf{c}, \mathbf{f})$ .
4. For all  $i \in T$  compute the error  $e_i = (u_i - f_i)^2$ .
5. For all  $i$  of the  $(1 - q) \cdot |T|$  largest values of  $\{e_i \mid i \in T\}$  reassign  $c_i := 1$ .
6. Remove the indices  $i \notin T$  from  $K$  and clear  $T$ .

while  $|K| > d \cdot |J|$ .

**Output:**

Pixel mask  $\mathbf{c}$ , such that  $\sum_{i \in J} c_i = d \cdot |J|$

---

The larger the parameters  $p$  and  $q$  are chosen, the faster the algorithm converges, since in each step,  $p \cdot q \cdot |K|$  pixels are removed. After  $k$  steps there are  $(1 - pq)^k \cdot |J|$  mask pixels left. Hence, for a density  $d$ , the algorithm terminates after at most  $\lceil \frac{\ln d}{\ln(1 - pq)} \rceil$  iterations, where  $\lceil \cdot \rceil$  denotes the ceiling function, giving the smallest integer not less than its argument.

Because there is a global interdependence between all selected mask pixels, probabilistic sparsification cannot guarantee to give optimal solutions. Therefore, the question arises how the parameters  $p$  and  $q$  influence the quality of the resulting mask. To this end, we run several experiments with different  $p$  and  $q$ . The results are depicted in Tab. 2. Note that we set the candidate set as well as the set of pixels that are removed to 1 if  $p$  or  $q$  would lead to sets smaller than one pixel. The optimal  $p$  is usually not very large: If too many candidates are removed from the mask, the local error does not provide enough information to select good pixels to remove permanently. The parameter  $q$  can usually be chosen as small as possible, i.e. such that only one candidate is removed in each iteration. For our test images, this was the case for  $q = 10^{-6}$ . With larger values for  $q$ , the probability that we remove important pixels increases.

Tab. 2 illustrates the robustness of the algorithm. Note that the approach is not deterministic and thus always returns different results since the candidates

**Table 2.** Influence of the parameters  $p$  and  $q$  of probabilistic sparsification. There have been in total 100 runs for each pair  $(p, q)$  on the test image *trui* with desired pixel density  $d = 0.04$ . Numbers in the table are the mean and standard deviation of the MSE. Again all pixel values lie in the interval  $[0, 255]$ .

$q$	$p$						
	0.01	0.02	0.05	0.1	0.2	0.3	0.4
$10^{-6}$	103.7 $\pm$ 1.88	98.2 $\pm$ 1.72	87.9 $\pm$ 1.61	77.6 $\pm$ 1.40	67.7 $\pm$ 1.40	<b>66.1 <math>\pm</math> 1.36</b>	70.7 $\pm$ 1.76
$10^{-3}$	103.7 $\pm$ 1.77	98.0 $\pm$ 1.87	87.7 $\pm$ 1.74	77.4 $\pm$ 1.33	67.8 $\pm$ 1.26	66.3 $\pm$ 1.41	70.5 $\pm$ 1.67
$10^{-2}$	103.1 $\pm$ 1.69	98.3 $\pm$ 1.91	88.9 $\pm$ 1.76	81.8 $\pm$ 1.68	73.0 $\pm$ 1.44	68.9 $\pm$ 1.81	69.4 $\pm$ 1.84
$2 \cdot 10^{-2}$	103.7 $\pm$ 1.99	98.7 $\pm$ 1.74	92.6 $\pm$ 1.57	85.3 $\pm$ 1.71	76.4 $\pm$ 1.78	71.4 $\pm$ 1.56	70.6 $\pm$ 1.83
$5 \cdot 10^{-2}$	104.9 $\pm$ 2.19	102.7 $\pm$ 1.96	98.1 $\pm$ 2.07	91.6 $\pm$ 1.82	82.7 $\pm$ 2.02	77.1 $\pm$ 2.03	74.6 $\pm$ 1.79
$10^{-1}$	110.3 $\pm$ 2.36	107.2 $\pm$ 2.63	103.7 $\pm$ 2.26	97.7 $\pm$ 2.14	89.5 $\pm$ 2.00	83.9 $\pm$ 2.22	80.8 $\pm$ 2.24

are chosen randomly at each iteration. Although the obtained masks for different seeds differ in most of the selected pixels, we obtain qualitatively comparable results: The standard deviation does not exceed a value of 2.6 and is even smaller for optimal values for  $p$  and  $q$ , when the algorithm is run several times.

In Fig. 8, the images in the third row show the results of the probabilistic sparsification for the test image *trui* with a mask pixel density of 4% ( $d = 0.04$ ). To optimise the quality, we use  $p = 0.3$  and  $q = 10^{-6}$  (cf. Tab. 2). Both the visual as well as the quantitative results outperform the ones of the analytic approach. This can also be observed for the two test images *walter* and *peppers*, as is shown in Tab. 4. The parameters  $p$  and  $q$  are optimised for each image individually.

**Nonlocal Pixel Exchange** As we have seen in the previous section, probabilistic sparsification outperforms the analytic approach. Nevertheless, it is not guaranteed to find an optimal solution. An obvious drawback of probabilistic sparsification is the fact that due to its greedy nature, once a point is removed, it will never be put back into the mask again. Thus, especially at later stages, where only few mask pixels are left, important points might have been removed, so that we end up in a suboptimal local minimum. We now present a method called nonlocal pixel exchange that allows to further improve the results of any previously obtained mask, in our case the one from probabilistic sparsification. It starts with a sparse, possibly suboptimal mask that contains already the desired density  $d$  of mask pixels. In each step, it randomly selects a set of  $m$  non-mask pixels as candidates. The candidate that exhibits the largest local error is then exchanged with a randomly chosen mask pixel. If the inpainting result with the new mask is worse than before, we revert the switch. Otherwise we proceed with the new mask. By construction, the nonlocal pixel exchange can only improve the result. This algorithm always converges towards an optimal solution in terms of a exchange of two

pixels. Since we exchange at each iteration the same number of candidate pixels it follows that this approach is not equivalent to an exhaustive search through all possible combinations. Thus, one cannot guarantee convergence towards the global minimum. The description below shows the details of the algorithm.

---

**Algorithm 5: Nonlocal Pixel Exchange**

---

**Input:**

Original image  $\mathbf{f}$ , pixel mask  $\mathbf{c}$ , size  $m$  of candidate set, the set  $K$  of pixel indices of the mask  $\mathbf{c}$ .

**Initialisation:**

$\mathbf{u} := r(\mathbf{c}, \mathbf{f})$  and  $\mathbf{c}^{\text{new}} := \mathbf{c}$ .

**Compute:**

Repeat

1. Choose randomly  $m \leq |K|$  pixel indices  $i$  from  $J \setminus K$  and compute the local error  $e_i := (u_i - f_i)^2$ .
2. Exchange step:  
Choose randomly a  $j \in K$  and set  $c_j^{\text{new}} := 0$ .  
For the largest value of  $e_i$ , set  $c_i^{\text{new}} := 1$ .
3. Compute  $\mathbf{u}^{\text{new}} := r(\mathbf{c}^{\text{new}}, \mathbf{f})$ .
4. If  $\text{MSE}(\mathbf{u}, \mathbf{f}) > \text{MSE}(\mathbf{u}^{\text{new}}, \mathbf{f})$   
     $\mathbf{u} := \mathbf{u}^{\text{new}}$  and  $\mathbf{c} := \mathbf{c}^{\text{new}}$ .  
    Update  $K$ .  
else  
    Reset  $\mathbf{c}^{\text{new}} := \mathbf{c}$ .

until no pairs can be found for exchange.

**Output:**

Optimised mask  $\mathbf{c}^{\text{new}}$ .

---

As for the previous algorithms, we are interested in an optimal parameter selection. Table 3 shows the results for different choices of  $m$  when the nonlocal pixel exchange is applied to the masks from the previous section (randomly selected, regular grid, and analytic approach from Fig. 8) and in addition the one we obtained by probabilistic sparsification (also Fig. 8). Technically one could always choose  $m = 1$ , but a noticeable speedup can be obtained by choosing a larger  $m$ . In our experiments, values around  $m = 20$  result in fastest convergence.

The nonlocal pixel exchange improves the masks from any method we have considered so far; see Fig. 7. Especially within the first few iterations we achieve significant quality gains. After 500,000 iterations, we reach with all three masks an MSE below 45. The best reconstruction with an MSE of 41.92 is obtained with the mask from probabilistic sparsification. It is depicted in Fig. 8. As for the previous methods, Tab. 4 provides also quantitative results for the test images *walter* and *peppers*. They support the above observations.

**Table 3.** Mean squared error after 500,000 iterations for different values for  $m$ , when the nonlocal pixel exchange is applied to different masks of the test image *trui* (see also Fig. 8). The best result for each mask is marked in boldface.

mask	$m$							
	1	5	10	20	30	40	50	100
randomly selected	49.88	46.43	44.99	<b>44.78</b>	45.00	45.07	45.25	48.22
regular grid	49.67	45.79	45.19	<b>44.76</b>	45.16	45.56	45.76	48.33
analytic approach	49.19	45.88	45.14	<b>44.70</b>	45.33	45.56	46.13	49.31
probabilistic sparsification	43.72	42.45	42.34	<b>41.92</b>	41.97	42.49	42.19	43.65

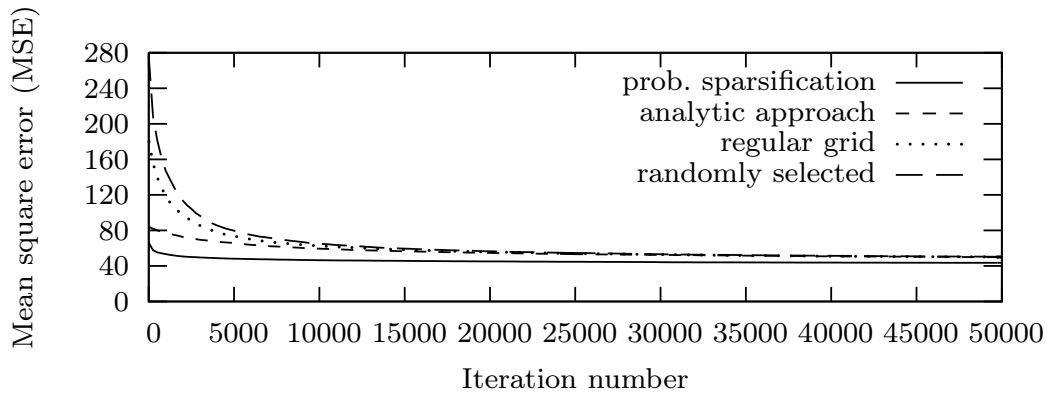


**Fig. 7.** Convergence behaviour for the first 50,000 iterations, when the nonlocal pixel exchange is applied to different masks (cf. Figure 8(a,d,g)) of the *trui* test image with optimal parameter  $m$  (cf. Table 3).

## 5.2 Optimising Tonal Data

So far, all our 2D optimisation approaches only propose a solution for the spatial optimisation problem. However, the results in Section 4.2 show that a tonal optimisation, i.e. an optimisation of the grey values, can be very worthwhile. From a data compression point of view, it is important to notice that changing the grey values at the chosen data points does not increase the amount of data that needs to be stored. The quality improvements, on the other hand, can be remarkable. In this section, we present an approach that allows us to determine the optimal grey values for any given mask.

In order to find the optimal grey values  $\mathbf{g}$  for a fixed mask  $\mathbf{c}$ , we consider the following minimisation approach:

$$\arg \min_{\mathbf{g}} \{ \|\mathbf{f} - \mathbf{r}(\mathbf{c}, \mathbf{g})\|^2 \}, \quad (29)$$

where  $\|\cdot\|$  is the standard Euclidean norm,  $\mathbf{f}$  denotes the original image, and  $\mathbf{r}(\mathbf{c}, \mathbf{g})$  the reconstruction from (28). Due to the linearity of  $\mathbf{r}$  with respect to  $\mathbf{g}$ , this is a linear least squares problem. In our next steps, we analyse its well-posedness properties and propose an efficient numerical algorithm.

**Existence and Uniqueness Results** Let  $\mathbf{e}_i$  denote the  $i$ -th canonical basis vector of  $\mathbb{R}^{|J|}$ , i.e.  $e_{i,j} = 1$  if  $i = j$ , and 0 otherwise. Then we call  $\mathbf{r}(\mathbf{c}, \mathbf{e}_i)$  the *inpainting echo* of pixel  $i$ . Since  $\mathbf{r}$  is linear in  $\mathbf{g}$  we can express the reconstruction  $\mathbf{u}$  as a superposition of its inpainting echoes:

$$\mathbf{u} = \mathbf{r}(\mathbf{c}, \mathbf{g}) = \mathbf{r}\left(\mathbf{c}, \sum_{i \in J} g_i \mathbf{e}_i\right) = \sum_{i \in J} g_i \mathbf{r}(\mathbf{c}, \mathbf{e}_i). \quad (30)$$

Since  $\mathbf{r}(\mathbf{c}, \mathbf{e}_i)$  is  $\mathbf{0}$  for  $c_i = 0$  (i.e. for  $i \in J \setminus K$ ), we can simplify this to a summation over  $K$ :

$$\mathbf{r}(\mathbf{c}, \mathbf{g}) = \sum_{i \in K} g_i \mathbf{r}(\mathbf{c}, \mathbf{e}_i). \quad (31)$$

For our minimisation problem (29), this means that the coefficients  $g_i$  can be chosen arbitrarily if  $i \in J \setminus K$ . For simplicity, we fix them at 0. The remaining  $g_i$  with  $i \in K$  can be obtained by considering the least squares problem

$$\arg \min_{\mathbf{g}_K} \{ \|\mathbf{B} \mathbf{g}_K - \mathbf{f}\|^2 \} \quad (32)$$

where  $\mathbf{g}_K = (g_i)_{i \in K}$  is a vector of size  $|K|$ , and  $\mathbf{B}$  is a  $|J| \times |K|$  matrix that contains the vectors  $\{\mathbf{r}(\mathbf{c}, \mathbf{e}_i) \mid i \in K\}$  as columns. The associated normal equations are given by

$$\mathbf{B}^\top \mathbf{B} \mathbf{g}_K = \mathbf{B}^\top \mathbf{f}. \quad (33)$$

By construction, the  $|K| \times |K|$  matrix  $\mathbf{B}^\top \mathbf{B}$  is positive semidefinite. It is, however, not obvious that the eigenvalue 0 cannot appear. The theorem below excludes such a singular situation.

**Theorem 3.** *Let  $K$  be nonempty. Then the matrix  $\mathbf{B}^\top \mathbf{B}$  is invertible, and thus the linear system (33) has a unique solution.*

*Proof.* Mainberger *et al.* [90] have proven that for a nonempty set  $K$ , the  $|J| \times |J|$  matrix  $\mathbf{M} = \mathbf{C} - (\mathbf{I} - \mathbf{C})\mathbf{A}$  is invertible, i.e.  $\mathbf{M}^{-1}$  exists. Moreover, for  $i \in K$  we have

$$\mathbf{r}(\mathbf{c}, \mathbf{e}_i) = \mathbf{M}^{-1} \mathbf{C} \mathbf{e}_i \stackrel{i \in K}{=} \mathbf{M}^{-1} \mathbf{e}_i. \quad (34)$$

This shows that  $\mathbf{r}(\mathbf{c}, \mathbf{e}_i)$  is the  $i$ -th column of  $\mathbf{M}^{-1}$ . Since  $\mathbf{M}$  is invertible, also  $\mathbf{M}^{-1}$  is regular. Thus, all column vectors of  $\mathbf{M}^{-1}$  have to be linearly independent. In particular, this implies that also all columns  $\{\mathbf{r}(\mathbf{c}, \mathbf{e}_i) \mid i \in K\}$  of the  $|J| \times |K|$  matrix  $\mathbf{B}$  are linearly independent. Therefore,  $\mathbf{B}^\top \mathbf{B}$  is invertible, and the linear system (33) has a unique solution.  $\square$

**Numerical Algorithm** To find the solution of the minimisation problem (29), Mainberger *et al.* [91] have solved the associated normal equations (33) iteratively. In particular, they have chosen a randomised Gauß-Seidel scheme that updates the grey values at the individual mask points one after another. Alternatively, one could also employ different iterative solvers or solve the system of equations with direct methods such as LU- or QR-decompositions [62]. In general, however, one has to state that typical methods which rely on inpainting echoes suffer from a relatively high computational cost to obtain the individual echoes. Although one can precompute and reuse them for the subsequent iteration steps, they still need to be computed at least once. This is particularly inefficient when a large amount of mask points is present. Moreover, precomputing inpainting echoes leads to higher memory requirements. The more recent strategies in [29, 64] avoid the direct computation of the inpainting echoes. Instead, the original minimisation problem (29) is solved directly with the help of primal-dual methods or related sophisticated optimisation strategies. This gives more efficient algorithms for tonal optimisation.

In the following, we propose an alternative approach to find optimal tonal data. It is based on an accelerated gradient descent strategy that allows an efficient grey value optimisation. Similar to [29, 64], we consider the original minimisation problem (29) directly. Thus, we also avoid computing inpainting echoes. This leads to a reduced runtime as well as to low memory requirements. Below we first explain the classical gradient method with exact line search. Afterwards we present a novel variant that benefits from an acceleration with a fast explicit diffusion scheme in the sense of Grewenig *et al.* [59].

Our goal is to minimise the objective function

$$E(\mathbf{g}) = \frac{1}{2} |\mathbf{r}(\mathbf{c}, \mathbf{g}) - \mathbf{f}|^2. \quad (35)$$

Starting with an initialisation  $\mathbf{g}^0 = \mathbf{C}\mathbf{f}$ , a gradient descent scheme minimises this energy  $E$  by iteratively updating the current grey values for  $k > 0$  as

$$\mathbf{g}^{k+1} = \mathbf{g}^k - \alpha \nabla E(\mathbf{g}^k) \quad (36)$$

with a step size  $\alpha$  and the gradient  $\nabla E(\mathbf{g}^k)$  depending on the iterates  $\mathbf{g}^k$ . Denoting the inpainting solution at iteration step  $k$  by  $\mathbf{u}^k$ , i.e.  $\mathbf{u}^k := \mathbf{r}(\mathbf{c}, \mathbf{g}^k)$ , the gradient can be written as

$$\nabla E(\mathbf{g}^k) = \mathbf{J}^\top (\mathbf{u}^k - \mathbf{f}) \quad (37)$$

where  $\mathbf{J}$  is the Jacobian of  $\mathbf{r}(\mathbf{c}, \mathbf{g}^k)$  with respect to the second component. With the definition of  $\mathbf{r}(\mathbf{c}, \mathbf{g}^k)$  from (28), we obtain

$$\begin{aligned} \mathbf{J}^\top &= \left( (\mathbf{C} - (\mathbf{I} - \mathbf{C})\mathbf{A})^{-1} \mathbf{C} \right)^\top \\ &= \mathbf{C} (\mathbf{C} - \mathbf{A}(\mathbf{I} - \mathbf{C}))^{-1} \end{aligned} \quad (38)$$

where we have exploited the symmetries of the matrices  $\mathbf{C}$  and  $\mathbf{A}$ . Computing the iterates  $\mathbf{u}^k$  and the gradient  $\nabla E(\mathbf{g}^k)$  means to solve a linear system of equations for each of them. This can be done efficiently with a bidirectional multigrid solver as is suggested in [90].

The main parameter that we have to specify is the step size  $\alpha$ . As one possibility, it can be optimised to yield the largest possible decay of the energy in each step. This comes down to the least squares problem

$$\arg \min_{\alpha > 0} \left\{ |\mathbf{f} - \mathbf{r}(\mathbf{c}, \mathbf{g}^k - \alpha \nabla E(\mathbf{g}^k))|^2 \right\}. \quad (39)$$

Exploiting the linearity of  $\mathbf{r}$  in the second component allows to obtain the minimiser in closed form:

$$\alpha = \frac{(\mathbf{f} - \mathbf{u}^k)^\top \mathbf{r}(\mathbf{c}, \nabla E(\mathbf{g}^k))}{|\mathbf{r}(\mathbf{c}, \nabla E(\mathbf{g}^k))|^2}. \quad (40)$$

This strategy is also known as exact line search. It guarantees that the sequence  $(\mathbf{g}^k)_k$  converges to the minimum of the energy [15]. As stopping criterion, we consider the relative norm of the gradient, which should approach zero at the optimum. In other words, we stop as soon as

$$|\nabla E(\mathbf{g}^k)|^2 \leq \varepsilon |\nabla E(\mathbf{g}^0)|^2 \quad (41)$$

with some small number  $\varepsilon > 0$ . An algorithmic overview of the classical gradient descent method with exact line search is shown below. It serves as our baseline method.



---

**Algorithm 6: Grey Value Optimisation with Exact Line Search**

---

**Input:**Original image  $\mathbf{f}$ , pixel mask  $\mathbf{c}$ .**Initialisation:**

$$\mathbf{g}^0 := \mathbf{C}\mathbf{f}, \quad k := 0.$$

**Compute:**Repeat for  $k \geq 0$ 

1. Compute the gradient

$$\nabla E(\mathbf{g}^k) := \mathbf{J}^\top \left( \mathbf{r}(\mathbf{c}, \mathbf{g}^k) - \mathbf{f} \right). \quad (42)$$

2. Determine the step size  $\alpha$  with Equation (40).
3. Update the tonal data:

$$\mathbf{g}^{k+1} := \mathbf{g}^k - \alpha \nabla E(\mathbf{g}^k). \quad (43)$$

until the stopping criterion (41) is fulfilled.

**Output:**Optimised grey values  $\mathbf{g}$ .

---

In order to speed up the gradient descent approach, we propose an accelerated algorithm based on a so-called *fast explicit diffusion (FED)* scheme. First applications of FED to image processing problems go back to Grewenig *et al.* [59]. FED can be used to speed up any explicit diffusion-like algorithm that involves a symmetric matrix. While classical explicit schemes employ a constant time step size that has to satisfy a restrictive stability limit, FED schemes involve cycles of time step sizes where up to 50 % of them can violate this stability limit. Nevertheless, at the end of each cycle, stability in the Euclidean norm is achieved. In contrast to classical explicit schemes that reach a stopping time of order  $O(M)$  in  $M$  steps, FED schemes with cycle length  $M$  progress to  $O(M^2)$ . This allows a very substantial acceleration.

Since the gradient descent scheme can be seen as an explicit scheme with a symmetric matrix, FED is applicable: If  $\alpha^*$  denotes a fixed step size for which (36) is stable in the Euclidean norm, one replaces it by the cyclically varying step sizes

$$\alpha_i = \alpha^* \cdot \frac{1}{2 \cos^2 \left( \pi \cdot \frac{2i+1}{4M+2} \right)} \quad (i = 0, \dots, M-1). \quad (44)$$

For large cycle lengths  $M$ , one should permute the order of the step sizes to tame rounding errors; see [133] for more details on this and an exhaustive explanation of the FED framework in general. The FED cycles should be iterated until the stopping criterion (41) is fulfilled. A related cyclic optimisation strategy has also been investigated in [120].

In order to determine the individual step sizes within each cycle, we have to find a step size  $\alpha^*$  that is within the stability limit. The following result is well-known in optimisation theory [99]: If  $E(\mathbf{g})$  is continuous and its gradient is Lipschitz continuous, i.e. there is a constant  $L$  such that

$$|\nabla E(\mathbf{g}_1) - \nabla E(\mathbf{g}_2)| \leq L \cdot |\mathbf{g}_1 - \mathbf{g}_2| \quad (45)$$

for all  $\mathbf{g}_1$  and  $\mathbf{g}_2$ , then the gradient descent scheme is stable for all step sizes  $\alpha^*$  fulfilling

$$0 < \alpha^* < \frac{2}{L}. \quad (46)$$

It is straightforward to verify that in our case  $L$  can be chosen as the squared spectral norm of the inpainting matrix  $\mathbf{D} := \mathbf{M}^{-1}\mathbf{C}$ , i.e.

$$L = \|\mathbf{D}\|^2 := \rho(\mathbf{D}^\top \mathbf{D}), \quad (47)$$

where  $\rho(\mathbf{D}^\top \mathbf{D})$  denotes the spectral radius of the symmetric matrix  $\mathbf{D}^\top \mathbf{D}$ . One possibility to estimate the spectral radius is to use Gershgorin's circle theorem. However, this may give a too pessimistic estimate. Instead, we propose to use the power method to determine the maximum eigenvalue of  $\mathbf{D}^\top \mathbf{D}$ ; see e.g. [2]. The convergence of this method turns out to be relatively fast, such that one obtains already a reasonable estimate of the spectral radius after 5 iterations.

Although it may appear tempting to choose  $\alpha^*$  close to the stability limit  $\frac{2}{L}$ , this can result in a suboptimal convergence speed, since high frequent error components are damped too slowly. Our experiments suggest that a good choice for  $\alpha^*$  is two third of the stability limit:

$$\alpha^* = \frac{4}{3L}. \quad (48)$$

Similar strategies are also common e.g. in multigrid approaches that use a damped Jacobi method with damping factor  $\frac{2}{3}$  as a baseline solver [17].

Below we give an algorithmic overview over all steps to perform tonal optimisation with FED-accelerated gradient descent:

---

### Algorithm 7: Grey Value Optimisation with FED

**Input:**

Original image  $\mathbf{f}$ , pixel mask  $\mathbf{c}$ , FED cycle length  $M$ .

**Initialisation:**

$\mathbf{g}^0 := \mathbf{C}\mathbf{f}$ ,  $k := 0$ .

**Compute:**

1. Estimate  $L$  in (47) with the power method.
2. Determine the FED time steps  $\alpha_0, \dots, \alpha_{M-1}$  according to (44) with  $\alpha^* = \frac{4}{3L}$ . If necessary, permute them.
3. Repeat for  $k \geq 0$

- (a)  $\mathbf{g}^{k,0} := \mathbf{g}^k$
- (b) For  $i = 0, \dots, M - 1$  do
  - i. Compute the gradient

$$\nabla E(\mathbf{g}^{k,i}) := \mathbf{J}^\top (\mathbf{r}(\mathbf{c}, \mathbf{g}^{k,i}) - \mathbf{f}). \quad (49)$$

- ii. Update the tonal data:

$$\mathbf{g}^{k,i+1} := \mathbf{g}^{k,i} - \alpha_i \nabla E(\mathbf{g}^{k,i}). \quad (50)$$

- (c)  $\mathbf{g}^{k+1} := \mathbf{g}^{k,M}$

until the stopping criterion (41) is fulfilled.

**Output:**

Optimised grey values  $\mathbf{g}$ .

Since the grey value optimisation problem is strictly convex, all convergent algorithms yield the same minimiser and are therefore qualitatively equivalent. They only differ by their run times. The following experiment gives an impression of realistic run times of both gradient descent algorithms for greyvalue optimisation. As before, we consider the inpainting problem with the test image *trui* ( $256 \times 256$  pixels) and 4 % mask density. The stopping parameter for our iterations was set to  $\varepsilon := 0.001$ . With a C implementation on a desktop PC with Intel Xeon processor (3.2GHz), the exact line search algorithm requires 458 seconds to perform 262 iterations. A corresponding FED algorithm with  $\alpha^* = 0.01$  needs only 77 seconds to compute 4 cycles of length  $M = 15$ . In comparison, a CPU implementation of the primal–dual approach of Hoeltgen and Weickert [64] requires for the same problem a run time of 346 seconds. This illustrates the favourable performance of the FED-accelerated gradient descent method.

As the FED algorithm is based on an explicit scheme, it is also well-suited for implementations on parallel hardware such as GPUs. This can lead to very substantial additional accelerations.

**Qualitative Evaluation** In order to evaluate the capabilities of the grey value optimisation, we apply it to the masks obtained so far for the test image *trui*. In all cases this results in a clear improvement of the reconstruction quality, both visually and in terms of their MSE; see Fig. 8 as well as Tab. 4. This confirms also our impressions from the 1D scenario in Section 4.2. Especially suboptimal masks benefit a lot from grey value optimisation: It can compensate for many deficiencies that are caused by an inferior spatial selection strategy. This becomes particularly apparent when considering the result for the random mask or the mask on the regular grid. It is remarkable how much gain in quality is possible by simply choosing different grey values. However, also the reconstruction we obtain with the best mask using probabilistic sparsification and nonlocal pixel exchange can

be improved substantially: The MSE is reduced from 41.92 to 27.24. Similar improvements can also be observed for the images *walter* and *peppers*; see Tab. 4. The best reconstructions are depicted in Fig. 6.

**Table 4.** Comparison of the reconstruction error (MSE) with 4% of all pixels for different test images and different inpainting data. The parameters were applied to both approaches, with and without grey value optimisation (GVO). The nonlocal pixel exchange was performed with  $5 \cdot 10^5$  iterations for each experiment.

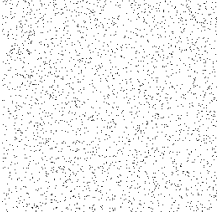


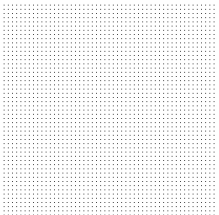


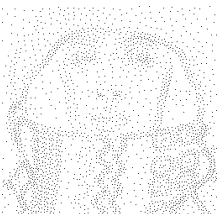
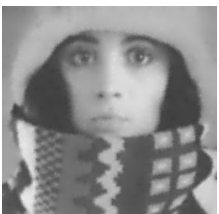
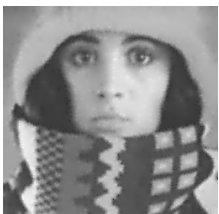
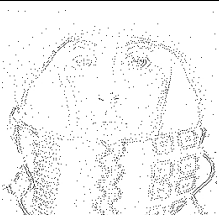


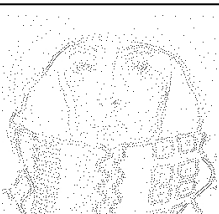
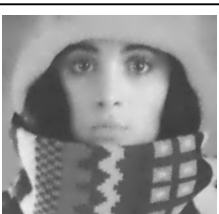
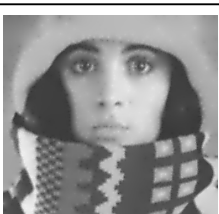
image	GVO	randomly selected	regular grid	analytic approach	probabilistic sparsification	nonlocal pixel exchange
<i>trui</i>	no	273.10	181.72	84.04	( $\sigma = 1.6,$ $s = 0.80$ )	41.92
	yes	151.25	101.62	42.00		<b>27.24</b> ( $m = 20$ )
<i>walter</i>	no	297.07	184.00	39.85	( $\sigma = 1.5,$ $s = 1.00$ )	18.37
	yes	155.50	91.97	20.19		<b>12.45</b> ( $m = 30$ )
<i>peppers</i>	no	278.61	185.04	70.05	( $\sigma = 1.5,$ $s = 0.95$ )	29.63
	yes	156.15	104.41	43.77		<b>25.10</b> ( $m = 30$ )

## 6 Extensions to Other Inpainting Operators

We have seen that optimising the interpolation data allows to obtain high quality reconstructions with only 4% of all pixels. These results are also remarkable in view of the fact that so far we have used a very simple interpolation operator: the Laplacian. It is unlikely that it offers the best performance. In this section we investigate the question if the algorithms of Section 5 can be used with, or extended to more advanced inpainting operators. We focus on two representative operators that have proven their good performance in the context of PDE-based image compression with sparse data [29, 53, 54, 118]: the biharmonic operator and the EED operator.

A straightforward extension of the Laplacian is the biharmonic operator, i.e. we replace  $\Delta u$  in (5) by  $-\Delta^2 u$ . Using it for interpolation comes down to thin plate spline interpolation [43], a rotationally invariant multidimensional generalisation of cubic spline interpolation. Compared to the Laplace operator, it yields a smoother solution  $u$  around the interpolation data, since its Green’s function is twice differentiable. This avoids the typical singularities that distort the visual quality with homogeneous diffusion inpainting. These artifacts are caused by the logarithmic singularities of the Green’s function of the two-dimensional Laplacian. On the other hand, biharmonic inpainting is prone to over- and undershoots, i.e. the values of  $u$  may leave the range of the inpainting data in  $K$ . This cannot happen for homogeneous diffusion inpainting which fulfils a maximum–minimum principle. Nevertheless, a number of evaluations show that biharmonic inpainting can offer a better reconstruction quality than homogeneous diffusion inpainting [29, 53, 54, 118].

Secondly we consider an anisotropic nonlinear diffusion operator, namely *edge enhancing-diffusion* (EED). Originally it has been introduced for image

	mask	reconstruction	reconstruction with optimal tonal data
random mask		 MSE: 273.10	 MSE: 151.25
regular grid		 MSE: 181.72	 MSE: 101.62
anal. approach		 MSE: 84.04	 MSE: 42.00
probab. sparsif.		 MSE: 66.11	 MSE: 36.04
nonl. pixel exch.		 MSE: 41.92	 MSE: 27.24

**Fig. 8.** Evaluation of different inpainting data using 4% of all pixels. **Left column:** Different masks obtained by using a regular grid, the analytic approach ( $s = 0.80$ ,  $\sigma = 1.6$ ), a probabilistic sparsification ( $p = 0.3$ ,  $q = 10^{-6}$ ), and with an additional nonlocal pixel exchange ( $m = 20$ ,  $5 \cdot 10^5$  iterations) after the previous probabilistic sparsification. **Middle column:** Reconstructions with homogeneous diffusion inpainting with the masks from the first column. **Right column:** Same as in the middle column, but with optimal tonal data.

denoising [131], and its application in image compression goes back to Galic *et al.* [53]. Using EED means that we replace  $\Delta u$  in (5) by  $\text{div}(\mathbf{D}(\nabla u_\sigma)\nabla u)$ . The positive definite matrix  $\mathbf{D}(\nabla u_\sigma)$  is the so-called diffusion tensor. It steers the diffusion process by its eigenvectors and eigenvalues. They depend on the gradient of a Gaussian-smoothed version  $u_\sigma$  of the image  $u$ , where  $\sigma$  denotes the standard deviation of the Gaussian. The first eigenvector of  $\mathbf{D}$  is chosen to be orthogonal to  $\nabla u_\sigma$ , and the corresponding eigenvalue is fixed at 1. This gives full diffusion / inpainting along image edges. In contrast, the second eigenvector is chosen to be parallel to  $\nabla u_\sigma$ , and its eigenvalue is a decreasing function of the local image contrast  $|\nabla u_\sigma|$ . Thus, one reduces diffusion / inpainting across high contrast edges. For image compression, one usually chooses the diffusivity of Charbonnier *et al.* [26], which is given by  $(1 + |\nabla u_\sigma|^2/\lambda^2)^{-1/2}$ . The parameter  $\lambda > 0$  allows to steer the contrast dependence.

Image inpainting with EED can reconstruct edges in high quality, even when the specified data is sparse [118]. This explains why EED has become one of the best performing operators for PDE-based image compression [53, 54, 118]. Moreover, for second order elliptic differential operators such as EED, the continuous theory guarantees a maximum–minimum principle [132]. Experiments show that in contrast to homogeneous diffusion inpainting, EED does not suffer from singularities [118].

What are the changes in our framework, when we replace the Laplacian by the biharmonic or the EED operator? If we discretise the biharmonic operator with central finite differences, we have to exchange the matrix  $\mathbf{A}$  in (7) by another constant matrix, but the structure of this equation remains the same as for homogeneous diffusion inpainting: It is a linear system of equations in the unknown vector  $\mathbf{u}$ . For EED, however, the discrete differential operator  $\mathbf{A}$  depends nonlinearly on the reconstruction  $\mathbf{u}$ . Thus, the resulting system of equations becomes nonlinear:

$$\mathbf{C}(\mathbf{u} - \mathbf{f}) - (\mathbf{I} - \mathbf{C})\mathbf{A}(\mathbf{u})\mathbf{u} = \mathbf{0}. \quad (51)$$

While this nonlinearity does not affect our spatial optimisation, we will see that it makes the tonal optimisation more difficult.

## 6.1 Optimising Spatial Data

Let us consider the spatial optimisation first. The theory behind the analytic approach is strongly based on homogeneous diffusion, and no extensions to more sophisticated inpainting operators have been discussed in [8]. Therefore, we do not consider this approach in this section.

In contrast, the probabilistic approach can be used without any restrictions and changes for both the biharmonic operator as well as for EED. As before, we search for the best parameters of the spatial optimisation methods. In all

our experiments, we fix the EED parameters to  $\lambda = 0.8$  and  $\sigma = 0.7$ , since this gives reconstructions of high quality.

Results for both operators and methods in comparison to homogeneous diffusion inpainting are shown in Tab. 5. Interestingly, the biharmonic operator does not achieve better results than the homogeneous one in the case of pure probabilistic sparsification without nonlocal pixel exchange. Our explanation for this observation is as follows: Biharmonic inpainting has a positive effect of increased smoothness around data points, and a negative effect by over- and undershoots in the inpainting domain. The latter one is ignored in the sparsification decision, since the point selection is based on a purely local error measurement. Thus, for very sparse data, over- and undershoots can become particularly detrimental on global error measures such as the MSE. In our experiment, the minimum and maximum values of the reconstruction lie around  $-59$  and  $346$ , respectively. This is far beyond the range of the original image which is given by [56, 214]. With an additional nonlocal pixel exchange, we can overcome this problem, since it uses the MSE as criterion to redistribute the mask pixels to more favourable locations. As a consequence, the grey value range of the reconstruction shrinks to the interval [47, 248], and the MSE falls from 79.26 to 20.89. This is far better than the MSE of 41.92 that we achieve for homogeneous diffusion inpainting.

However, EED with probabilistic sparsification gives far superior results. Already without nonlocal pixel exchange, we obtain an MSE of 24.20. Post-processing with nonlocal pixel exchange reduces the error to only 12.62.

Figures 9(a) and (c) depict the masks obtained with probabilistic sparsification combined with the nonlocal pixel exchange for both operators. Comparing them with the one from homogeneous diffusion inpainting (see Fig. 8), we observe interesting differences: Homogeneous diffusion inpainting requires more pixels near edges to represent these discontinuities well. Thus, for a specified pixel number, it has less pixels to approximate the interior of the regions. This explains why biharmonic or EED inpainting can achieve lower errors.

**Table 5.** Comparison of the reconstruction error (MSE) with 4% of all pixels for different inpainting operators and different data optimisation algorithms. The parameters were applied to both approaches, with and without grey value optimisation (GVO). The nonlocal pixel exchange was performed with  $5 \cdot 10^5$  iterations for each experiment.

operator	reg. grid	probab. sparsif.	nonl. pixel exch.	with GVO
homogeneous	181.72	66.11 ( $p = 0.3, q = 10^{-6}$ )	41.92 ( $m = 20$ )	<b>27.24</b>
biharmonic	107.96	79.26 ( $p = 0.005, q = 10^{-6}$ )	20.89 ( $m = 10$ )	<b>16.73</b>
EED ( $\lambda = 0.8, \sigma = 0.7$ )	102.85	24.20 ( $p = 0.05, q = 10^{-6}$ )	12.62 ( $m = 30$ )	<b>10.79</b>

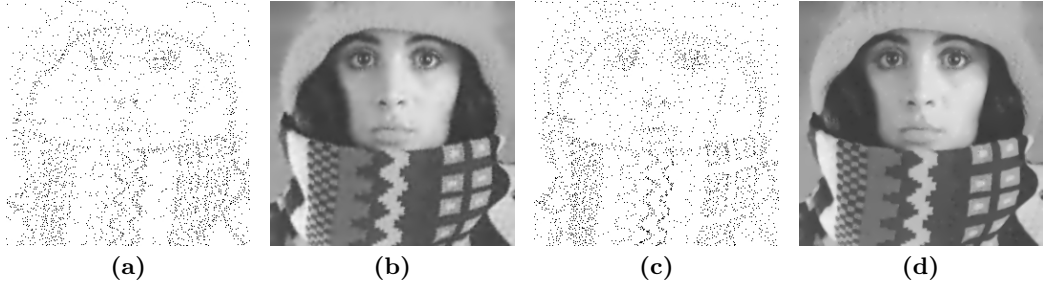


**Fig. 9.** Best mask and reconstruction for the biharmonic operator (a, b) and EED (c, d) for the test image *trui* with 4 % of all pixels, using probabilistic sparsification, nonlocal pixel exchange, and tonal optimisation. The image (b) has an MSE of 16.73, while image (d) has an MSE of 10.79. Parameters have been chosen as in Table 5.

## 6.2 Optimising Tonal Data

We have seen that for homogeneous diffusion inpainting, an additional tonal optimisation yields significant improvements in the reconstruction quality. Thus, we should also investigate if it is beneficial for biharmonic and EED inpainting.

In the case of biharmonic inpainting, our tonal optimisation strategy from Subsection 5.2 carries over literally, since we are still facing a linear least squares problem: For a fixed inpainting mask, the reconstruction depends linearly of the specified grey values. Thus, all we have to do is to exchange the discrete differential operator for homogeneous diffusion inpainting by its biharmonic counterpart. Also our algorithms such as the FED-accelerated gradient descent remain applicable. The final results for biharmonic inpainting with spatial and tonal optimisation are listed in Tab. 5, and the best reconstruction is depicted in Fig. 9(b). As one can see, tonal optimisation allows to reduce the MSE from 20.89 to 16.73.

Since our tonal optimisation methods are tailored towards linear least squares formulations, specific challenges arise when we want to extend them to EED-based inpainting. The nonlinearity of the EED inpainting scheme prevents closed form expressions such as (37) and (38). This is caused by the fact that the matrix  $\mathbf{A}$  is now a function of the inpainted image  $\mathbf{u}^k$ , which itself depends on the grey value data  $\mathbf{g}^k$  in the specified pixels. Although this concatenated mapping is formally smooth, one should keep in mind that EED has the ability to create edge-like structures. This means that in practice the problem is fairly ill-conditioned: Small local changes in  $\mathbf{g}^k$  may have a strong global impact on  $\mathbf{u}^k$ , on  $\mathbf{A}(\mathbf{u}^k)$ , and on the Jacobian of the error function (35). Moreover, there is no guarantee anymore that the tonal optimisation problem is strictly convex. Thus, it may have many local minimisers. It is therefore not surprising that different algorithms and even different parameter settings within the same algorithm may end up in different minimisers. Since it is difficult to design practically feasible algorithms that guarantee to find the global minimiser, we focus on transparent and conceptually simple local



optimisation strategies such as gradient descent. We have done a number of experiments with several variants of gradient descent approaches for tonal optimisation in EED-based inpainting. Below we describe the method that has yielded the best results in terms of reconstruction quality.

We suggest to modify the gradient descent approach for (35) as follows. While we keep the basic structure of (36) and (37), we lack a closed form solution of type (38) for the Jacobian  $\mathbf{J}$  that is now an unknown function of the evolving grey value data  $\mathbf{g}^k$ . As a remedy, we approximate the Jacobian by numerical differentiation:

$$(\mathbf{J}(\mathbf{g}^k))_{i,j} := \frac{\mathbf{r}(\mathbf{c}, \mathbf{g}^k + \eta \mathbf{e}_j)_i - \mathbf{r}(\mathbf{c}, \mathbf{g}^k)_i}{\eta}, \quad (52)$$

where  $i$  denotes the pixel index,  $j$  is the index of an individual mask point, and the parameter  $\eta > 0$  quantifies a small grey value perturbation at the mask point  $j$ . As before,  $\mathbf{e}_j$  is the canonical basis vector with a unit impulse in pixel  $j$ . Note that the grey values at all non-mask points do not have any influence on the inpainting result. Thus, the Jacobian does not have to be computed for those locations.

In contrast to our linear grey value optimisation strategies, we abstain from adapting the gradient descent step size  $\alpha$  by means of exact line search or cyclic FED-based variations: We have experienced that the high sensitivity of the Jacobian w.r.t.  $\mathbf{g}^k$  suggests to keep the gradient descent step size  $\alpha$  fairly small to capture this dynamics in an adequate way. On the other hand, too small values for  $\alpha$  can also result in a convergence towards a fairly poor local minimiser. Thus, in practice, one fixes  $\alpha$  to some small value.

Similar considerations apply to the parameter  $\eta$  in (52): The nonlinear dynamics of the Jacobian suggests to use small values for  $\eta$  in order to approximate the derivative well. On the other side, if  $\eta$  is too small, numerical problems can arise, since both the numerator and the denominator in (52) approach zero.

Table 6 shows how an appropriate selection of the parameters  $\alpha$  and  $\eta$  can be used to optimise the reconstruction quality for EED-based inpainting. We observe that in our test scenario the resulting tonal optimisation step allows to reduce the MSE from 12.62 to 10.79. The corresponding reconstruction is depicted in Fig. 9(d). Tab. 5 shows that the MSE of 10.79 obtained for EED is far better than the errors for homogeneous diffusion inpainting (MSE=27.24) and for biharmonic inpainting (MSE=16.73). To the best of our knowledge, such a reconstruction quality has never been achieved before for PDE-based inpainting with a mask density of only 4%.

## 7 Summary and Conclusions

The contributions of our work are twofold: On the one hand we gave a comprehensive survey on the state-of-the-art in PDE-based image compression.

**Table 6.** MSE obtained after a tonal optimisation for the EED inpainting approach with the final mask from Fig. 9. The parameter  $\alpha$  denotes the fixed step size in each gradient descent iteration, and  $\eta$  is the step size used for the computation of the derivatives by means of finite differences.

$\eta$	$\alpha$	
	$10^{-3}$	$10^{-2}$
1.0	10.86	<b>10.79</b>
1.5	10.93	10.80
2.0	10.88	10.80
3.0	10.88	10.81

It enables the readers to obtain an overview of the achievements that have been made in this field and guide them to the relevant literature.

On the other hand, we were focusing on one key problem in PDE-based image compression: the spatial and tonal data optimisation. Here we aimed at obtaining insights into the full potential of the quality gains, without imposing any constraints on the type of inpainting operator, the computational costs, or the coding costs for the optimised data. Our strategy was to start with more restricted settings that allow a deeper understanding of the problem, and to extend our findings to more general scenarios afterwards.

In the 1D setting, we restricted ourselves to homogeneous diffusion inpainting of strictly convex functions. For the resulting free knot problem for linear spline interpolation, we came up with a new algorithm and discussed optimal approximation results. We showed the nonconvexity of the problem for more than three knots, and we saw that a splitting into a spatial optimisation step followed by a tonal one does not deteriorate the reconstruction quality substantially.

This motivated us to use such a splitting strategy also for the 2D setting and without restrictions on the convexity or concavity of the image data. For spatial data optimisation with homogeneous diffusion inpainting, we studied a probabilistic sparsification approach with nonlocal pixel exchange in detail. For the subsequent tonal optimisation step we established the existence of a unique solution. We showed that it can be found efficiently with a gradient descent approach which is accelerated by a fast explicit diffusion (FED) strategy.

In our investigations we were aiming at fairly generic algorithms that can also be applied to other inpainting operators such as biharmonic inpainting and inpainting based on edge-enhancing anisotropic diffusion (EED). Data optimisation for EED-based inpainting allowed us to come up with reconstructions of hitherto unparalleled quality.

Our framework for data optimisation permits to specify the desired mask density *a priori*. This is a conceptual advantage over approaches that have to tune a regularisation parameter in order to influence the density which

results *a posteriori* [29, 63]. In practice this means that the latter approaches may have to run the algorithm many times.

While our results show the large potential of PDE-based inpainting, it should be emphasised that data optimisation is a key problem, but not the only one that must be solved for building well-performing codecs: For example, both the location and the grey values of the data must be stored efficiently, and some real-world applications require very fast algorithms. This poses additional constraints and challenges that will be addressed in our forthcoming publications.

*Acknowledgements* Our research is partly funded by the Deutsche Forschungsgemeinschaft (DFG) through a Gottfried Wilhelm Leibniz Prize. This is gratefully acknowledged. We also thank Pascal Gwosdek and Christian Schmaltz for providing the electrostatic halftoning images for us.

## Bibliography

- [1] Acar, T., Gökmen, M.: Image coding using weak membrane model of images. In: A.K. Katsaggelos (ed.) *Visual Communications and Image Processing '94, Proceedings of SPIE*, vol. 2308, pp. 1221–1230. SPIE Press, Bellingham (1994)
- [2] Allaire, G., Trabelsi, K., Kaber, S.: *Numerical Linear Algebra. Texts in Applied Mathematics*. Springer, New York (2008)
- [3] Alter, F., Durand, S., Froment, J.: Adapted total variation for artifact free decompression of JPEG images. *Journal of Mathematical Imaging and Vision* **23**(2), 199–211 (2005)
- [4] Arigovindan, M., Sühling, M., Hunziker, P., Unser, M.: Variational image reconstruction from arbitrarily spaced samples: A fast multiresolution spline solution. *IEEE Transactions on Image Processing* **14**(4), 450–460 (2005)
- [5] Azzam, A., Kreyszig, E.: On solutions of elliptic equations satisfying mixed boundary conditions. *SIAM Journal of Mathematical Analysis* **13**(2), 254–262 (1982)
- [6] Bae, E., Weickert, J.: Partial differential equations for interpolation and compression of surfaces. In: M. Daehlen, M. Floater, T. Lyche, J.L. Merrien, K. Mørken, L.L. Schumaker (eds.) *Mathematical Methods for Curves and Surfaces, Lecture Notes in Computer Science*, vol. 5862, pp. 1–14. Springer, Berlin (2010)
- [7] Bastani, V., Helfroush, M., Kasiri, K.: Image compression based on spatial redundancy removal and image inpainting. *Journal of Zhejiang University – Science C (Computers & Electronics)* **11**(2), 92–100 (2010)
- [8] Bellhachmi, Z., Bucur, D., Burgeth, B., Weickert, J.: How to choose interpolation data in images. *SIAM Journal on Applied Mathematics* **70**(1), 333–352 (2009)
- [9] Bertalmío, M., Sapiro, G., Caselles, V., Ballester, C.: Image inpainting. In: *Proc. SIGGRAPH 2000*, pp. 417–424. New Orleans, LI (2000)
- [10] Blu, T., Thévenaz, P., Unser, M.: Linear interpolation revitalized. *IEEE Transactions on Image Processing* **13**(5), 710–719 (2004)
- [11] de Boor, C.: Good approximation by splines with variable knots II. In: G. Watson (ed.) *Conference on the Numerical Solution of Differential Equations, Lecture Notes in Mathematics*, vol. 363, pp. 12–20. Springer (1974)
- [12] Bornemann, F., März, T.: Fast image inpainting based on coherence transport. *Journal of Mathematical Imaging and Vision* **28**(3), 259–278 (2007)

- [13] Bougleux, S., Peyré, G., Cohen, L.: Image compression with anisotropic triangulations. In: Proc. Tenth International Conference on Computer Vision, pp. 2343–2348. Kyoto, Japan (2009)
- [14] Bourquard, A., Unser, M.: Anisotropic interpolation of sparse generalized image samples. *IEEE Transactions on Image Processing* **22**(2), 459–472 (2013)
- [15] Boyd, S., Vandenberghe, L.: *Convex Optimization*. Cambridge University Press, Cambridge (2004)
- [16] Bredies, K., Holler, M.: A total variation-based JPEG decompression model. *SIAM Journal on Imaging Sciences* **5**(1), 366–393 (2012)
- [17] Briggs, W.L.: *A Multigrid Tutorial*. SIAM, Philadelphia (1987)
- [18] Brinkmann, E., Burger, M., Grah, I.: Regularization with sparse vector fields: From image compression to TV-type reconstruction. In: J. Aujol, M. Nikolova, N. Papadakis (eds.) *Scale Space and Variational Methods in Computer Vision, Lecture Notes in Computer Science*, vol. 9087, pp. 191–202. Springer, Berlin (2015)
- [19] Brown, R.: The mixed problem for Laplace’s equation in a class of Lipschitz domains. *Communications in Partial Differential Equations* **19**(7–8), 1217–1233 (1994)
- [20] Buhmann, M.D.: *Radial Basis Functions*. Cambridge University Press, Cambridge, UK (2003)
- [21] Carlsson, S.: Sketch based coding of grey level images. *Signal Processing* **15**, 57–83 (1988)
- [22] Caselles, V., Morel, J.M., Sbert, C.: An axiomatic approach to image interpolation. *IEEE Transactions on Image Processing* **7**(3), 376–386 (1998)
- [23] Catté, F., Lions, P.L., Morel, J.M., Coll, T.: Image selective smoothing and edge detection by nonlinear diffusion. *SIAM Journal on Numerical Analysis* **32**, 1895–1909 (1992)
- [24] Chan, T.F., Shen, J.: Non-texture inpainting by curvature-driven diffusions (CDD). *Journal of Visual Communication and Image Representation* **12**(4), 436–449 (2001)
- [25] Chan, T.F., Zhou, H.M.: Total variation improved wavelet thresholding in image compression. In: Proc. Seventh International Conference on Image Processing, vol. II, pp. 391–394. Vancouver, Canada (2000)
- [26] Charbonnier, P., Blanc-Féraud, L., Aubert, G., Barlaud, M.: Deterministic edge-preserving regularization in computed imaging. *IEEE Transactions on Image Processing* **6**(2), 298–311 (1997)
- [27] Chen, J., Ye, F., Di, J., Liu, C., Men, A.: Depth map compression via edge-based inpainting. In: Proc. 2012 Picture Coding Symposium, pp. 57–60. Kraków, Poland (2012)
- [28] Chen, S.: Image reconstruction from zero-crossings. In: Proc. Eighth International Joint Conference on Artificial Intelligence, vol. 2, pp. 742–744. Milan, Italy (1987)

- [29] Chen, Y., Ranftl, R., Pock, T.: A bi-level view of inpainting-based image compression. In: Z. Kúkelová, J. Heller (eds.) Proc. 19th Computer Vision Winter Workshop. Křtiny, Czech Republic (2014)
- [30] Cohen, A., Dyn, N., Hecht, F., Mirebeau, J.: Adaptive multiresolution analysis based on anisotropic triangulations. *Mathematics of Computation* **81**(278), 789–810 (2012)
- [31] Cox, M.G.: An algorithm for approximating convex functions by means of first degree splines. *The Computer Journal* **14**(3), 362–364 (1971)
- [32] Curtis, S.R., Oppenheim, A.V., Lim, J.S.: Reconstruction of two-dimensional signals from threshold crossings. In: Proc. IEEE International Conference on Acoustics, Speech and Signal Processing, vol. 10, pp. 1057–1060. Tampa, FL (1985)
- [33] D’Angelo, E., Jacques, L., Alahi, A., Vandergheynst, P.: From bits to images: Inversion of local binary descriptors. *IEEE Transactions on Pattern Analysis and Machine Intelligence* **36**(5), 874–887 (2014)
- [34] Davis, P.J.: *Interpolation and Approximation*. Blaisdell Publishing Company (1963)
- [35] Demaret, L., Dyn, N., Iske, A.: Image compression by linear splines over adaptive triangulations. *Signal Processing* **86**(7), 1604–1616 (2006)
- [36] Desai, U.Y., Mizuki, M.M., Masaki, I., Horn, B.K.P.: Edge and mean based image compression. Tech. Rep. 1584 (A.I. Memo), Artificial Intelligence Lab., Massachusetts Institute of Technology, Cambridge, MA (1996)
- [37] DeVore, R.A., Popov, V.A.: Free multivariate splines. *Constructive Approximation* **3**, 239–248 (1987)
- [38] Di Blasi, G., Francomano, E., Tortorici, A., Toscano, E.: A smoothed particle image reconstruction method. *Calcolo* **48**(1), 61–74 (2011)
- [39] Dikoussar, N.D., Török, C.: Data smoothing by splines with free knots. *Physics of Particles and Nuclei Letters* **5**(3), 324–327 (2008)
- [40] Distasi, R., Nappi, M., Vitulano, S.: Image compression by B-tree triangular coding. *IEEE Transactions on Communications* **45**(9), 1095–1100 (1997)
- [41] Doshkov, D., Ndjiki-Nya, P., Lakshman, H., Köppel, M., Wiegand, T.: Towards efficient intra prediction based on image inpainting methods. In: Proc. 28th Picture Coding Symposium, pp. 470–473. Nagoya, Japan (2010)
- [42] Dron, L.: The multiscale veto model: A two-stage analog network for edge detection and image reconstruction. *International Journal of Computer Vision* **11**(1), 45–61 (1993)
- [43] Duchon, J.: Interpolation des fonctions de deux variables suivant le principe de la flexion des plaques minces. *RAIRO Analyse Numérique* **10**(3), 5–12 (1976)

- [44] Dyn, N., Levin, D., Rippa, S.: Data dependent triangulations for piecewise linear interpolation. *IMA Journal of Numerical Analysis* **10**(1), 137–154 (1990)
- [45] Elder, J.H.: Are edges incomplete? *International Journal of Computer Vision* **34**(2/3), 97–122 (1999)
- [46] Elder, J.H., Goldberg, R.M.: Image editing in the contour domain. *IEEE Transactions on Pattern Analysis and Machine Intelligence* **23**(3), 291–296 (2001)
- [47] Facciolo, G., Arias, P., Caselles, V., Sapiro, G.: Exemplar-based interpolation of sparsely sampled images. In: D. Cremers, Y. Boykov, A. Blake, F. Schmidt (eds.) *Energy Minimisation Methods in Computer Vision and Pattern Recognition, Lecture Notes in Computer Science*, vol. 5681, pp. 331–344. Springer, Berlin (2009)
- [48] Facciolo, G., Lecumberry, F., Almansa, A., Pardo, A., Caselles, V., Rougé, B.: Constrained anisotropic diffusion and some applications. In: *Proc. 2006 British Machine Vision Conference*, vol. 3, pp. 1049–1058. Edinburgh, Scotland (2006)
- [49] Faille, F., Petrou, M.: Invariant image reconstruction from irregular samples and hexagonal grid splines. *Image and Vision Computing* **28**(8), 1173–1183 (2010)
- [50] Fichera, G.: Analisi esistenziale per le soluzioni dei problemi al contorno misti, relativi all equazione e ai sistemi di equazioni del secondo ordine di tipo ellittico, autoaggiunti. *Annali della Scuola Normale Superiore di Pisa — Classe di Scienze* **3**(1), 75–100 (1949)
- [51] Floyd, R.W., Steinberg, L.: An adaptive algorithm for spatial grey scale. *Proceedings of the Society of Information Display* **17**, 75–77 (1976)
- [52] Ford, G.E.: Application of inhomogeneous diffusion to image and video coding. In: *Proc. 13th Asilomar Conference on Signals, Systems and Computers*, vol. 2, pp. 926–930. Asilomar, CA (1996)
- [53] Galić, I., Weickert, J., Welk, M., Bruhn, A., Belyaev, A., Seidel, H.P.: Towards PDE-based image compression. In: N. Paragios, O. Faugeras, T. Chan, C. Schnörr (eds.) *Variational, Geometric and Level-Set Methods in Computer Vision, Lecture Notes in Computer Science*, vol. 3752, pp. 37–48. Springer, Berlin (2005)
- [54] Galić, I., Weickert, J., Welk, M., Bruhn, A., Belyaev, A., Seidel, H.P.: Image compression with anisotropic diffusion. *Journal of Mathematical Imaging and Vision* **31**(2–3), 255–269 (2008)
- [55] Gautier, J., Le Meur, O., Guillemot, C.: Efficient depth map compression based on lossless edge coding and diffusion. In: *Proc. 2012 Picture Coding Symposium*, pp. 81–84. Kraków, Poland (2012)
- [56] Gilbarg, D., Trudinger, N.: *Elliptic Partial Differential Equations of Second Order*. Springer, Berlin (2001)

- [57] Gomathi, R., Kumar, A.V.A.: A multiresolution image completion algorithm for compressing digital color images. *Journal of Applied Mathematics* **2014**, Article ID 757,318 (2014)
- [58] Grattoni, P., Guiducci, A.: Contour coding for image description. *Pattern Recognition Letters* **11**(2), 95–105 (1990)
- [59] Grewenig, S., Weickert, J., Bruhn, A.: From box filtering to fast explicit diffusion. In: M. Goesele, S. Roth, A. Kuijper, B. Schiele, K. Schindler (eds.) *Pattern Recognition, Lecture Notes in Computer Science*, vol. 6376, pp. 533–542. Springer, Berlin (2010)
- [60] Grossauer, H., Scherzer, O.: Using the complex Ginzburg–Landau equation for digital inpainting in 2D and 3D. In: L.D. Griffin, M. Lillholm (eds.) *Scale-Space Methods in Computer Vision, Lecture Notes in Computer Science*, vol. 2695, pp. 225–236. Springer, Berlin (2003)
- [61] Hamideh, H.: On the optimal knots of first degree splines. *Kuwait Journal of Science and Engineering* **29**(1), 1–13 (2002)
- [62] Higham, N.J.: *Accuracy and Stability of Numerical Algorithms*, 2nd edn. SIAM, Philadelphia (2002)
- [63] Hoeltgen, L., Setzer, S., Weickert, J.: An optimal control approach to find sparse data for Laplace interpolation. In: A. Heyden, F. Kahl, C. Olsson, M. Oskarsson, X.C. Tai (eds.) *Energy Minimisation Methods in Computer Vision and Pattern Recognition, Lecture Notes in Computer Science*, vol. 8081, pp. 151–164. Springer, Berlin (2013)
- [64] Hoeltgen, L., Weickert, J.: Why does non-binary mask optimisation work for diffusion-based image compression? In: X.C. Tai, E. Bae, T.F. Chan, S.Y. Leung, M. Lysaker (eds.) *Energy Minimisation Methods in Computer Vision and Pattern Recognition, Lecture Notes in Computer Science*, vol. 8932, pp. 85–98. Springer, Berlin (2015)
- [65] Hoffmann, S., Mainberger, M., Weickert, J., Puhl, M.: Compression of depth maps with segment-based homogeneous diffusion. In: A. Kuijper, K. Bredies, T. Pock, H. Bischof (eds.) *Scale Space and Variational Methods in Computer Vision, Lecture Notes in Computer Science*, vol. 7893, pp. 319–330. Springer, Berlin (2013)
- [66] Hoffmann, S., Plonka, G., Weickert, J.: Discrete Green’s functions for harmonic and biharmonic inpainting with sparse atoms. In: X.C. Tai, E. Bae, T.F. Chan, M. Lysaker (eds.) *Energy Minimization Methods in Computer Vision and Pattern Recognition, Lecture Notes in Computer Science*, vol. 8932, pp. 169–182. Springer, Berlin (2015)
- [67] Horn, B., Schunck, B.: Determining optical flow. *Artificial Intelligence* **17**, 185–203 (1981)
- [68] Huffman, D.A.: A method for the construction of minimum redundancy codes. *Proceedings of the IRE* **40**, 1098–1101 (1952)
- [69] Hummel, R., Moniot, R.: Reconstructions from zero-crossings in scale space. *IEEE Transactions on Acoustics, Speech, and Signal Processing* **37**, 2111–2130 (1989)



- [70] Jeschke, S., Cline, D., Wonka, P.: Estimating color and texture parameters for vector graphics. *Computer Graphics Forum* **30**(2), 523–532 (2011)
- [71] Johansen, P., Skelboe, S., Grue, K., Andersen, J.D.: Representing signals by their topoints in scale space. In: *Proc. Eighth International Conference on Pattern Recognition*, pp. 215–217. Paris, France (1986)
- [72] Joint Bi-level Image Experts Group: Information technology – progressive lossy/lossless coding of bi-level images. ISO/IEC JTC1 11544, ITU-T Rec. T.82 (1993). Final Committee Draft 11544
- [73] Jupp, D.L.B.: Approximation to data by splines with free knots. *SIAM Journal on Numerical Analysis* **15**(2), 328–343 (1978)
- [74] Kanters, F.M.W., Lillholm, M., Duits, R., Jansen, B.J.P., Platel, B., Florack, L.M.J., ter Haar Romeny, B.M.: On image reconstruction from multiscale top points. In: R. Kimmel, N. Sochen, J. Weickert (eds.) *Scale Space and PDE Methods in Computer Vision, Lecture Notes in Computer Science*, vol. 3459, pp. 431–439. Springer, Berlin (2005)
- [75] Kazinnik, R., Dekel, S., Dyn, N.: Low bit-rate image coding using adaptive geometric piecewise polynomial approximation. *IEEE Transactions on Image Processing* **16**(9), 2225–2233 (2007)
- [76] Kioustelidis, J.B., Spyropoulos, K.J.:  $L_1$  approximation of strictly convex functions by means of first degree splines. *Computing* **20**(1), 35–45 (1978)
- [77] Kohout, J.: On digital image representation by the Delaunay triangulation. In: D. Mery, L. Rueda (eds.) *Advances in Image and Video Technology, Lecture Notes in Computer Science*, vol. 4872, pp. 826–840. Springer, Berlin (2007)
- [78] Kopilovic, I., Szirányi, T.: Artifact reduction with diffusion preprocessing for image compression. *Optical Engineering* **44**(2), 1–14 (2005)
- [79] Köstler, H., Stürmer, M., Freundl, C., Rüde, U.: PDE based video compression in real time. Tech. Rep. 07–11, Lehrstuhl für Informatik 10 (Systemsimulation), Friedrich–Alexander–Universität Erlangen–Nürnberg, Germany (2007)
- [80] Kurt, B., Gökmen, M., Jain, A.: Image compression based on Centripede Model. In: A. Del Bimbo (ed.) *Image Analysis and Processing, Lecture Notes in Computer Science*, vol. 1310, pp. 303–310. Springer, Berlin (1997)
- [81] Ladyženskaja, O.A., Ural’ceva, N.N.: *Linear and Quasilinear Elliptic Equations*. Academic Press (1968)
- [82] Lehner, B., Umlauf, G., Hamann, B.: Image compression using data-dependent triangulations. In: G. Bebis, R. Boyle, B. Parvin, D. Koracin, N. Paragios, S. Tanveer, T. Ju, Z. Liu, S. Coquillart, C. Cruz-Neira, T. Müller, T. Malzbender (eds.) *Advances in Visual Computing, Lecture Notes in Computer Science*, vol. 4841, pp. 351–362. Springer, Berlin (2007)

- [83] Li, X.: Anisotropic mesh adaptation for image representation and scaling. arXiv:1402.4893v1 [cs.CV] (2014)
- [84] Li, Y., Sjostrom, M., Jennehag, U., Olsson, R.: A scalable coding approach for high quality depth image compression. In: Proc. 3DTV-Conference: The True Vision – Capture, Transmission and Display of 3D Video. IEEE, Zurich, Switzerland (2012)
- [85] Lillholm, M., Nielsen, M., Griffin, L.D.: Feature-based image analysis. *International Journal of Computer Vision* **52**(2/3), 73–95 (2003)
- [86] Liu, D., Sun, X., Wu, F.: Inpainting with image patches for compression. *Journal of Visual Communication and Image Representation* **23**(1), 100–113 (2012)
- [87] Liu, D., Sun, X., Wu, F., Li, S., Zhang, Y.Q.: Image compression with edge-based inpainting. *IEEE Transactions on Circuits, Systems and Video Technology* **17**(10), 1273–1286 (2007)
- [88] Logan, Jr., B.F.: Information in the zero crossings of bandpass signals. *Bell System Technical Journal* **56**, 487–510 (1977)
- [89] Mahoney, M.: Data compression programs. <http://mattmahoney.net/dc/> (2009). Last visited November 30, 2009
- [90] Mainberger, M., Bruhn, A., Weickert, J., Forchhammer, S.: Edge-based image compression of cartoon-like images with homogeneous diffusion. *Pattern Recognition* **44**(9), 1859–1873 (2011)
- [91] Mainberger, M., Hoffmann, S., Weickert, J., Tang, C.H., Johannsen, D., Neumann, F., Doerr, B.: Optimising spatial and tonal data for homogeneous diffusion inpainting. In: A.M. Bruckstein, B. ter Haar Romeny, A.M. Bronstein, M.M. Bronstein (eds.) *Scale Space and Variational Methods in Computer Vision, Lecture Notes in Computer Science*, vol. 6667, pp. 26–37. Springer, Berlin (2012)
- [92] Mainberger, M., Schmaltz, C., Berg, M., Weickert, J., Backes, M.: Diffusion-based image compression in steganography. In: G. Bebis, R. Boyle, B. Parvin, D. Koracin, C. Fowlkes, S. Wang, M. Choi, S. Mantler, J. Schulze, D. Acevedo, K. Mueller, M. Papka (eds.) *Advances in Visual Computing, Part II, Lecture Notes in Computer Science*, vol. 7432, pp. 447–457. Springer, Berlin (2012)
- [93] Mallat, S., Zhong, S.: Characterisation of signals from multiscale edges. *IEEE Transactions on Pattern Analysis and Machine Intelligence* **14**, 720–732 (1992)
- [94] Masnou, S., Morel, J.M.: Level lines based disocclusion. In: Proc. 1998 IEEE International Conference on Image Processing, vol. 3, pp. 259–263. Chicago, IL (1998)
- [95] Miranda, C.: Sul problema misto per le equazioni lineari ellittiche. *Annali di Matematica Pura ed Applicata* **39**, 279–303 (1955)
- [96] Miranda, C.: *Partial Differential Equations of Elliptic Type*, 2nd edn. Springer, Berlin (1970)

- [97] Moinard, M., Amonou, I., Brault, P., Duhamel, P.: Image and video compression scheme based on the prediction of transformed coefficients. In: Proc. Seventh International Symposium on Image and Signal Processing and Analysis, pp. 385–389. Dubrovnik, Croatia (2011)
- [98] Morton, K.W., Mayers, L.M.: Numerical Solution of Partial Differential Equations, 2nd. edn. Cambridge University Press, Cambridge, UK (2005)
- [99] Nesterov, Y., Nesterov, I.: Introductory Lectures on Convex Optimization: A Basic Course. Applied Optimization. Springer, Berlin (2004)
- [100] Nürnberger, G., Braess, D.: Nonuniqueness of best  $L_p$ -approximation for generalized convex functions by splines with free knots. Numerical Functional Analysis and Optimization **4**(2), 199–209 (1982)
- [101] Ochs, P., Chen, Y., Brox, T., Pock, T.: iPiano: Inertial proximal algorithm for nonconvex optimization. SIAM Journal on Imaging Sciences **7**, 1388–1419 (2014)
- [102] Olsen, S., Gooch, B.: Image simplification and vectorization. In: Proc. ACM SIGGRAPH/Eurographics Symposium on Non-Photorealistic Animation and Rendering, pp. 65–74. Vancouver, BC, Canada (2011)
- [103] Orzan, A., Bousseau, A., Winnemöller, H., Barla, P., Thollot, J., Salesin, D.: Diffusion curves: A vector representation for smooth-shaded images. ACM Transactions on Graphics **27**(3), Article No. 92 (2008)
- [104] Pennebaker, W.B., Mitchell, J.L.: JPEG: Still Image Data Compression Standard. Springer, New York (1992)
- [105] Perona, P., Malik, J.: Scale space and edge detection using anisotropic diffusion. IEEE Transactions on Pattern Analysis and Machine Intelligence **12**, 629–639 (1990)
- [106] Peter, P., Schmaltz, C., Mach, N., Mainberger, M., Weickert, J.: Beyond pure quality: Progressive mode, region of interest coding and real time video decoding in PDE-based image compression. Tech. Rep. 354, Department of Mathematics, Saarland University, Saarbrücken, Germany (2015)
- [107] Peter, P., Weickert, J.: Colour image compression with anisotropic diffusion. In: Proc. 21st IEEE International Conference on Image Processing, pp. 4822–4826. Paris, France (2014)
- [108] Peter, P., Weickert, J.: Compressing images with diffusion- and exemplar-based inpainting. In: J. Aujol, M. Nikolova, N. Papadakis (eds.) Scale Space and Variational Methods in Computer Vision, *Lecture Notes in Computer Science*, vol. 9087, pp. 154–165. Springer, Berlin (2015)
- [109] Phillips, G.M.: Algorithms for piecewise straight line approximations. The Computer Journal **11**(2), 211–212 (1968)
- [110] Plonka, G., Hoffmann, S., Weickert, J.: Pseudo-inverses of difference matrices and their application to sparse signal approximation. arXiv:1504.04266 [math.NA] (2015)

- [111] Rane, S.D., Sapiro, G., Bertalmío, M.: Structure and texture filling-in of missing image blocks in wireless transmission and compression applications. *IEEE Transactions on Image Processing* **12**(3), 296–302 (2003)
- [112] Rice, J.R.: *The Approximation of Functions – Volume 1: Linear Theory*, 1 edn. Addison-Wesley (1964)
- [113] Rodrigues, M., Osman, A., Robinson, A.: Partial differential equations for 3D data compression and reconstruction. *Advances in Dynamical Systems and Applications* **8**(2), 303–315 (2013)
- [114] Rudin, L.I., Osher, S., Fatemi, E.: Nonlinear total variation based noise removal algorithms. *Physica D* **60**, 259–268 (1992)
- [115] Saloma, C., Haeberli, P.: Two-dimensional image reconstruction from Fourier coefficients computed directly from zero crossings. *Applied Optics* **32**(17), 3092–3093 (1993)
- [116] Schmaltz, C., Gwosdek, P., Bruhn, A., Weickert, J.: Electrostatic halftoning. *Computer Graphics Forum* **29**(8), 2313–2327 (2010)
- [117] Schmaltz, C., Mach, N., Mainberger, M., Weickert, J.: Progressive modes in PDE-based image compression. In: *Proc. 30th Picture Coding Symposium*, pp. 233–236. IEEE, San Jose, CA (2013)
- [118] Schmaltz, C., Peter, P., Mainberger, M., Ebel, F., Weickert, J., Bruhn, A.: Understanding, optimising, and extending data compression with anisotropic diffusion. *International Journal of Computer Vision* **108**(3), 222–240 (2014)
- [119] Schmaltz, C., Weickert, J.: Video compression with 3-D pose tracking, PDE-based image coding, and electrostatic halftoning. In: A. Pinz, T. Pock, H. Bischof, F. Leberl (eds.) *Pattern Recognition, Lecture Notes in Computer Science*, vol. 7476, pp. 438–447. Springer, Berlin (2012)
- [120] Setzer, S., Steidl, G., Morgenthaler, J.: On cyclic gradient descent reprojection. *Computational Optimization and Applications* **54**(2), 417–440 (2013)
- [121] Solé, A., Caselles, V., Sapiro, G., Arandiga, F.: Morse description and geometric encoding of digital elevation maps. *IEEE Transactions on Image Processing* **13**(9), 1245–1262 (2004)
- [122] Solin, P., Andrs, D.: On scientific data and image compression based on adaptive higher-order FEM. *Advances in Applied Mathematics and Mechanics* **1**(1), 56–68 (2009)
- [123] Stone, H.: Approximation of curves by line segments. *Mathematics of Computation* **15**(73), 40–47 (1961)
- [124] Strobach, P.: Quadtree-structured recursive plane decomposition coding of images. *IEEE Transactions on Signal Processing* **39**(6), 1380–1397 (1991)
- [125] Sullivan, G.J., Baker, R.J.: Efficient quadtree coding of images and video. *IEEE Transactions on Image Processing* **3**(3), 327–331 (1994)

- [126] Taubman, D.S., Marcellin, M.W. (eds.): *JPEG 2000: Image Compression Fundamentals, Standards and Practice*. Kluwer, Boston (2002)
- [127] Tschumperlé, D.: Fast anisotropic smoothing of multi-valued images using curvature-preserving PDE's. *International Journal of Computer Vision* **68**(1), 65–82 (2006)
- [128] Tsuji, H., Sakatani, T., Yashima, Y., Kobayashi, N.: A nonlinear spatio-temporal diffusion and its application to prefiltering in MPEG-4 video coding. In: *Proc. 2002 IEEE International Conference on Image Processing*, vol. 1, pp. 85–88. Rochester, NY (2002)
- [129] Uhlir, K., Skala, V.: Reconstruction of damaged images using radial basis functions. In: *Proc. 13th European Signal Processing Conference (EUSIPCO)*, pp. 160–163. Antalya, Turkey (2005)
- [130] Wang, C., Sun, X., Wu, F., Xiong, H.: Image compression with structure-aware inpainting. In: *Proc. 2006 IEEE International Symposium on Circuits and Systems*, pp. 1816–1819. Kos, Greece (2006)
- [131] Weickert, J.: Theoretical foundations of anisotropic diffusion in image processing. *Computing Supplement* **11**, 221–236 (1996)
- [132] Weickert, J.: *Anisotropic Diffusion in Image Processing*. Teubner, Stuttgart (1998)
- [133] Weickert, J., Grewenig, S., Schroers, C., Bruhn, A.: Cyclic schemes for PDE-based image analysis. Technical Report 327, Department of Mathematics, Saarland University, Saarbrücken, Germany (2015)
- [134] Weickert, J., Welk, M.: Tensor field interpolation with PDEs. In: J. Weickert, H. Hagen (eds.) *Visualization and Processing of Tensor Fields*, pp. 315–325. Springer, Berlin (2006)
- [135] Weinzaepfel, P., Jégou, H., Pérez, P.: Reconstructing an image from its local descriptors. In: *Proc. 2011 IEEE Computer Society Conference on Computer Vision and Pattern Recognition*, pp. 337–344. IEEE Computer Society Press, Colorado Springs, CO (2011)
- [136] Werner, H.: Studies on contour: I. qualitative analyses. *The American Journal of Psychology* **47**(1), 40–64 (1935)
- [137] Wu, Y., Zhang, H., Sun, Y., Guo, H.: Two image compression schemes based on image inpainting. In: *Proc. 2009 International Joint Conference on Computational Sciences and Optimization*, pp. 816–820. Sanya, China (2009)
- [138] Xie, Z., Franklin, W.R., Cutler, B., Andrade, M.A., Inanc, M., Tracy, D.M.: Surface compression using over-determined Laplacian approximation. In: F.T. Luk (ed.) *Advanced Signal Processing Algorithms, Architectures, and Implementations XVII, Proceedings of SPIE*, vol. 6697. SPIE Press, Bellingham (2007)
- [139] Xiong, Z.W., Sun, X.Y., Wu, F., Li, S.P.: Image coding with parameter-assistant inpainting. In: *Proc. 2007 IEEE International Conference on Image Processing*, vol. 2, pp. 369–372. San Antonio, TX (2007)

- [140] Yatnalli, V., Sudha, K.L.: Image compression with inpainting. In: Proc. IEEE International Symposium on Signal Processing and Information Technology, pp. 158–163. Ho Chi Minh City, Vietnam (2012)
- [141] Zaremba, S.: Sur un problème mixte relatif à l'équation de Laplace. Bulletin International de l'Académie des Sciences de Cracovie pp. 313–344 (1910)
- [142] Zeevi, Y., Rotem, D.: Image reconstruction from zero-crossings. IEEE Transactions on Acoustics, Speech, and Signal Processing **34**, 1269–1277 (1986)
- [143] Zhao, C., Du, M.: Image compression based on PDEs. In: Proc. 2011 International Conference of Computer Science and Network Technology, pp. 1768–1771. Harbin, China (2011)